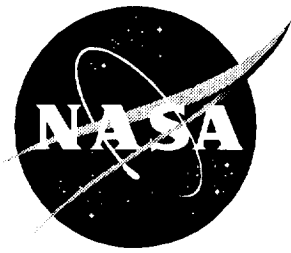


NASA Technical Memorandum 4714

Artificial Boundary Conditions for Computation of Oscillating External Flows

S. V. Tsynkov

August 1996



NASA Technical Memorandum 4714

Artificial Boundary Conditions for Computation of Oscillating External Flows

S. V. Tsynkov
Langley Research Center • Hampton, Virginia

National Aeronautics and Space Administration
Langley Research Center • Hampton, Virginia 23681-0001

August 1996

Acknowledgments

I am very thankful to V. S. Ryaben'kii of the Keldysh Institute for Applied Mathematics, Russian Academy of Sciences, whose ideas constitute the foundation of our joint research in numerical methods for external problems and who influenced much of the content of this paper. S. Abarbanel of the School of Mathematical Sciences, Tel-Aviv University, is acknowledged for his valuable help in formulating the problem and for numerous useful discussions. I would also like to thank V. Matsaev and E. Shustin of the School of Mathematical Sciences, Tel-Aviv University, and D. Gottlieb of the Division of Applied Mathematics, Brown University, for their helpful comments. The suggestions of H. Atkins, T. Roberts, and C. Swanson of the NASA Langley Research Center have contributed much to the improvement of this paper.

Available electronically at the following URL address: <http://techreports.larc.nasa.gov/ltrs/ltrs.html>

Printed copies available from the following:

NASA Center for AeroSpace Information
800 Elkridge Landing Road
Linthicum Heights, MD 21090-2934
(301) 621-0390

National Technical Information Service (NTIS)
5285 Port Royal Road
Springfield, VA 22161-2171
(703) 487-4650

Abstract

In this paper, we propose a new technique for the numerical treatment of external flow problems with oscillatory behavior of the solution in time. Specifically, we consider the case of unbounded compressible viscous plane flow past a finite body (airfoil). Oscillations of the flow in time may be caused by the time-periodic injection of fluid into the boundary layer, which in accordance with experimental data, may essentially increase the performance of the airfoil. To conduct the actual computations, we have to somehow restrict the original unbounded domain, that is, to introduce an artificial (external) boundary and to further consider only a finite computational domain. Consequently, we will need to formulate some artificial boundary conditions (ABC's) at the introduced external boundary. The ABC's we are aiming to obtain must meet a fundamental requirement. One should be able to uniquely complement the solution calculated inside the finite computational domain to its infinite exterior so that the original problem is solved within the desired accuracy. Our construction of such ABC's for oscillating flows is based on an essential assumption: the Navier-Stokes equations can be linearized in the far field against the free-stream background. To actually compute the ABC's, we represent the far-field solution as a Fourier series in time and then apply the Difference Potentials Method (DPM) of V. S. Ryaben'kii. This paper contains a general theoretical description of the algorithm for setting the DPM-based ABC's for time-periodic external flows. Based on our experience in implementing analogous ABC's for steady-state problems (a simpler case), we expect that these boundary conditions will become an effective tool for constructing robust numerical methods to calculate oscillatory flows.

1. Introduction

The numerical study of problems originally formulated on unbounded domains requires the implementation of special techniques for the “treatment of infinity” (which is necessitated by the restricted facilities of modern computers). One of the corresponding techniques is based on an artificial truncation of the original infinite domain, which implies that one must set special boundary conditions at the external (artificial) boundary of the newly formed finite computational domain. The aim of this paper is to describe the theoretical foundations for constructing such artificial boundary conditions (ABC's) for the computation of certain unsteady external flows.

Before proceeding to the actual description of the problem, let us first define the concept of *exact ABC's*. Namely, exact ABC's are the boundary conditions that enable one to uniquely complement the solution of the “truncated problem” to the unbounded exterior of the computational domain so that the original problem is solved. The exact ABC's usually appear to be nonlocal for steady-state problems in space and for time-dependent problems in both space and time.

Let us emphasize that our main objective in this paper is to construct special boundary conditions that would model (and in the ideal case equivalently replace) the exterior part of the problem, i.e., the part we eliminate by truncation. Many examples of such boundary conditions can be found in comprehensive reviews by Givoli. (See refs. 1 and 2.) This formulation differs from another well-known problem related to setting the boundary conditions for numerical algorithms, namely, to construct such boundary conditions that would ensure well-posedness of the truncated problem and stability of the

integration process in time. In fact, these two formulations are not completely independent. For example, the issue of well-posedness for certain classes of (local) ABC's was thoroughly investigated by Gustafsson. (See refs. 3–5.) On the other hand, a group of very delicate questions related to the issue of long-time stability is studied by Carpenter, Gottlieb, and Abarbanel in reference 6 (for some specific boundary-value problems). The issue of connections between the (highly accurate nonlocal) boundary conditions that “model the infinity” and the boundary conditions that ensure the long-time stability will be an interesting subject for a future investigation.

In this paper, we consider an unbounded compressible viscous flow past a finite body or configuration of bodies (e.g., single-element or multi-element airfoil). The behavior of the flow in time is assumed to be oscillatory. We must emphasize that while talking about the oscillatory time behavior we mean that some alternating (time-periodic) influence is exerted on the flow (e.g., see experimental work by Seifert, et al. in ref. 7) and expect that those frequencies that are connected to this influence will dominate in the solution. We expect that this circumstance will enable us to construct the ABC's without taking into account any other time-dependent effects. From a mathematical standpoint, this case fills an intermediate position between the steady-state and true unsteady flows.

The steady-state case is relatively simple compared with time-dependent flows. In reference 8, we have constructed the ABC's for calculating external viscous compressible steady-state flows. These boundary conditions were based on the concept of far-field linearization and on the application of the Difference Potentials Method (DPM) of Ryaben'kii. (See refs. 9 and 10.) The ABC's (ref. 8) differ only slightly from the exact ABC's (a more rigorous formulation of the latter statement may be found in ref. 8); therefore, the ABC's (ref. 8) turn out to be global in space. However, practical implementation of these boundary conditions is fairly easy. (See refs. 11 and 12.) They were used along with the Navier-Stokes code by Jameson, Schmidt, Turkel, and Swanson (refs. 13–15) for computing different external flows. Numerical experiments show that the global DPM-based ABC's (ref. 8) provide high accuracy of computations, as well as fast convergence of the multigrid iteration procedure to a steady state. (See refs. 11 and 12.) The computational cost of boundary conditions (refs. 8, 11, and 12) is not high in comparison with the total cost of the original procedure. (See refs. 13–15.) Generally, the numerical algorithm we used for integrating the Navier-Stokes equations became more robust (in comparison with the standard procedure (refs. 13–15)) if supplemented by the DPM-based ABC's. (See ref. 8.)

Additionally, we would like to emphasize that the ABC's (ref. 8) were constructed specially for the steady-state problem and on the basis of stationary governing equations, independent of any specific technique for solving the stationary equations inside the computational domain. In practical computations, we use multigrid iterations (refs. 13–15) for calculating the steady-state solutions in references 11 and 12. In doing so, we set the ABC's (ref. 8) on each iteration on the upper time level. Of course, the boundary data on the intermediate stage of the iteration procedure (i.e., until we achieve the steady state) are not necessarily consistent with the formal “stationary” treatment of the far field. However, treating the “time-intermediate” boundary data as if it were already steady has been found effective in computational practice. (See refs. 11 and 12.) We are going to use a similar idea for the time-periodic case studied in this paper.

True unsteady flows are much more complicated in terms of both theoretical analysis and practical calculations. In general, the exact ABC's for unsteady problems will be nonlocal in both space and time. Therefore, the corresponding computational cost may appear to be rather high. This is also true for the global DPM-based boundary conditions which can be constructed as close to the exact ones as desired. The corresponding general theory for unsteady problems is contained in work by Ryaben'kii. (See ref. 16.)

However, an intermediate case of oscillatory time behavior must be less expensive in terms of required computer resources since the global character of the ABC's in time will obviously be restricted by the value of one period. Moreover, the theoretical analysis of this case based on the usage of

the Fourier representation in time also appears to be less complicated than the general one from reference 16 since in our analysis we actually reduce the time-dependent problem to a family of steady-state problems.

On the other hand, don't assume that the oscillating flow is a particular and, therefore, an unimportant case. For example, experiments (ref. 7) show that the time-periodic injection of fluid into the turbulent boundary layer may increase its resistance to adverse pressure gradients without separation. This implies an essential improvement of airfoil performance, up to 60 percent for high (post stall) angles of attack, according to reference 7. The phenomenon was observed on different geometries (original NACA0015 airfoil, the same airfoil with the deflected flap, and some others), which leads us to believe that it may be effectively used in aircraft design. Therefore, an accurate numerical investigation of the phenomenon becomes an important issue, and an accurate procedure for setting the ABC's must be one of the principle elements of any computational algorithm used for such an investigation.

The previous example is probably not a unique one where the time-periodic treatment of flow in the far field might be relevant. In general, for the oscillatory case we propose the following construction of ABC's. First, linearize the governing equations in the far field. Then, assuming that the time period is initially prescribed, apply the Fourier transform in time and obtain a family of steady-state problems (where the unknowns are amplitudes). The latter problems are then treated by means of the DPM. (See refs. 9 and 10.) The central idea of the DPM-based approach is to equivalently replace the problem formulated on a domain by a certain operator equation formulated on its boundary. For each one of the foregoing steady-state problems (note, the family of these problems is parameterized by the frequency, i.e., by the dual Fourier variable), this replacement results in an operator equation formulated at the artificial boundary of the computational domain (i.e., connecting the boundary values of the solution). The operator involved (a projection) is somewhat analogous to the boundary pseudodifferential operators introduced by Calderon. (See ref. 17.) Because of the equivalence to the exterior linear problem, the previously-mentioned operator equation (more precisely, the entire family of these equations) can be considered a desirable exact ABC (limited only by the accuracy of far-field linearization) for the problem solved inside the computational domain. In other words, this operator equation adequately takes into account the structure of the solution from outside the computational domain, which might also be called *the exact transfer of boundary conditions from infinity*. (See ref. 16.)

We actually develop the DPM-based ABC's for the already discrete formulation of the problem. In doing so, the set of the frequencies involved is obviously finite. Therefore, we can actually compute the corresponding boundary operator for each one of the steady-state problems arising after the Fourier transform in time. Then, for reasons of numerical convenience, we represent the solution to the linearized exterior problem in the form of generalized potential. (See refs. 9 and 10.) The density of generalized potential serves as an unknown function in the previously-mentioned operator equation. By using the generalized potential to set the ABC's we gain more generality from a geometric standpoint. Moreover, we can easily match the solutions of the interior nonlinear problem and the exterior linear problem when conducting practical computations. (We need to actually calculate the generalized potential only in some neighborhood of the computational domain, to be discussed later.) Finally, applying the inverse Fourier transform, we obtain ABC's in a matrix form, which enables easy practical implementation. In fact, the entire procedure may be thought of as solving the linearized problem outside the computational domain and then using the obtained solution to close the "truncated system" that is solved inside the computational domain.

To conclude this introduction, let us point out an analogy to the previously investigated steady-state case. (See ref. 8.) Namely, we are looking here for a solution to the unsteady problem that is defined on an initially prescribed time interval (one period) and that meets the periodicity condition in time (at least in the far field). To develop the ABC's for this case, we solve a certain linear problem in the far field (by means of the DPM). The latter problem is also formulated for the time interval of one period. The ABC's for the time-periodic case are basically constructed independent of any specific technique for

integrating the Navier-Stokes equations inside the computational domain (as the ABC's (ref. 8) were constructed irrespective of any specific way for actual computation of the steady state). Based on the assumption of periodicity in time, these boundary conditions simply close the system that is solved inside the computational domain; the closure is constructed for the time interval of one period. In practice, however, achieving the true oscillatory regime may require long-time computational runs that cover many periods. During this long-time integration, each moment we need to update the external boundary data using the ABC's (i.e., each time step) we treat the flow as it were already time-periodic (in some generalized sense, see section 3). In so doing, the boundary conditions should guarantee only the desirable far-field behavior of the solution. This behavior is actually determined by the condition that all perturbations vanish at infinity (as in refs. 8, 11, and 12 when we were treating the external boundary data on each iteration as already steady and demanding that the ABC's ensure the decrease of the solution to the linearized problem at infinity).

This paper is organized as follows. In section 2, we describe the basic formulations of the problems. Specifically, in subsection 2.1 we describe a geometric setup typical for the numerical solution of external flow problems, i.e., configurations of the finite computational domain and its infinite exterior. In this subsection, we also introduce the flow equations (parabolized Navier-Stokes) and linearize them in the far field against the constant free-stream background. In so doing, we obtain a coupled problem, which is nonlinear inside the finite computational domain and linear outside it. Then, assuming that the period of oscillating motion is known, we Fourier transform the exterior linear system with respect to time and obtain an equivalent family of steady-state systems. These steady-state systems must be solved as a part of the solution to the aforementioned coupled problem. However, we do not solve them directly since the corresponding domain is still infinite. Instead, we equivalently replace each of the exterior linear steady-state systems by the generalized Calderon pseudodifferential equation formulated at the external boundary of the computational domain. To calculate the pseudodifferential operation (projection) we need a special auxiliary problem that is first formulated on the entire plane for the linearized thin-layer equations (after the Fourier transform in time) with a certain compactly supported right-hand side. Solvability of this auxiliary problem (in the sense of tempered distributions) is studied in subsection 2.2. Then, in subsection 2.3, we show how one can replace the original auxiliary problem formulated on an unbounded domain (entire plane) by a new problem formulated on some rectangle so that the solutions of the two problems are in a certain sense close to each other.

Section 3 of this paper is devoted to numerics. In subsection 3.1, we introduce a finite-difference scheme that approximates the linearized thin-layer equations. Since we discretize the equations not only in space but also in time, we now get a finite (discrete) series instead of the original infinite Fourier series which implies that the family of steady-state systems to be solved outside the computational domain becomes finite as well. In subsection 3.2, we construct a difference analogue to the auxiliary problem on the rectangle, describe the numerical algorithm for its solution (referring to our previous work for some details) and briefly address our somewhat non-standard concept of convergence for the solutions of the difference auxiliary problem. Finally, in subsection 3.3 we show how one uses the recently formulated difference auxiliary problem and obtains difference analogue to the Calderon boundary pseudodifferential projection. Using this difference boundary projection and also calculating the generalized difference potential, we actually compute the nonlocal DPM-based ABC's. The ABC's are first obtained in the Fourier variables and then, after implementing the inverse transform, in the physical variables as well. Finally, section 4 contains some conclusions and possible generalizations.

2. Basic Formulations

2.1. Governing Equations and Geometric Setup

Let us start with the parabolized Navier-Stokes equations, which are the same as the thin-layer equations for two dimensions (see ref. 18 by Anderson, Tannehill, and Pletcher):

$$\left. \begin{aligned}
\frac{\partial \rho}{\partial t} + \frac{\partial \rho u}{\partial x} + \frac{\partial \rho v}{\partial y} &= 0 \\
\rho \frac{\partial u}{\partial t} + \rho u \frac{\partial u}{\partial x} + \rho v \frac{\partial u}{\partial y} + \frac{\partial p}{\partial x} &= \frac{1}{Re} \frac{\partial}{\partial y} \mu \frac{\partial u}{\partial y} \\
\rho \frac{\partial v}{\partial t} + \rho u \frac{\partial v}{\partial x} + \rho v \frac{\partial v}{\partial y} + \frac{\partial p}{\partial y} &= \frac{1}{Re} \frac{4}{3} \frac{\partial}{\partial y} \mu \frac{\partial v}{\partial y} \\
\rho \frac{\partial \varepsilon}{\partial t} + \rho u \frac{\partial \varepsilon}{\partial x} + \rho v \frac{\partial \varepsilon}{\partial y} + p \left(\frac{\partial u}{\partial x} + \frac{\partial v}{\partial y} \right) &= \frac{1}{Re} \left[\mu \left(\frac{\partial u}{\partial y} \right)^2 + \frac{4}{3} \mu \left(\frac{\partial v}{\partial y} \right)^2 + \frac{\gamma}{Pr} \frac{\partial}{\partial y} \mu \frac{\partial \varepsilon}{\partial y} \right]
\end{aligned} \right\} \quad (1)$$

Here, x and y denote the Cartesian coordinates, u and v denote the Cartesian velocity projections, ρ denotes the density, p denotes the pressure, ε denotes the internal energy, μ denotes the viscosity, and γ denotes the ratio of specific heats. To derive the last of equations (1), we assume that the gas is perfect and that the Prandtl number $Pr = \mu c_p / \kappa$ is constant (κ is the heat conduction coefficient). We denote the free-stream parameters, specifically, u_0 , v_0 , p_0 , ρ_0 , ε_0 , and μ_0 , by the subscript "0." We additionally assume that $v_0 = 0$ and $u_0 > 0$, which does not imply any loss of generality. The system (1) is written in dimensionless form. The following scales were used to obtain dimensionless quantities: u_0 was used for velocity; ρ_0 for density, $\rho_0 u_0^2$ for pressure, u_0^2 for internal energy, μ_0 for viscosity, characteristic size L (typically, airfoil chord) for all distances, and L/u_0 for time. The factor $1/Re$ that multiplies the viscous terms in equations (1) arises from the nondimensionalization. Here, $Re = \frac{\rho_0 u_0 L}{\mu_0}$ is the Reynolds number.

Note that in our previous work (refs. 8, 11, and 12) we used the full Navier-Stokes equations to construct the ABC's for steady-state problems. In this paper, we are going to use the thin-layer system (eqs. (1)). This system appears to apply quite well to the description of certain viscous flows (ref. 18), in particular, the far-field flows that we are studying hereafter. Moreover, for the thin-layer system (eqs. (1)) we can justify some results on the solvability of its linearized counterpart on R^2 , which is important for the general justification of our construction of ABC's. Finally, the usage of equations (1) instead of the full Navier-Stokes equations may save an appreciable amount of computer resources, as will be seen from further consideration.

Let us now assume that the actual values of u , v , p , ρ , ε , and μ in the far field only slightly deviate from the corresponding free-stream parameters. For dimensionless quantities, this means

$$\left. \begin{aligned}
\rho &= 1 + \tilde{\rho} & u &= 1 + \tilde{u} & v &= \tilde{v} & \mu &= 1 + \tilde{\mu} & p &= (\gamma M_0^2)^{-1} + \tilde{p} \\
\varepsilon &= [(\gamma - 1)\gamma M_0^2]^{-1} + \tilde{\varepsilon}
\end{aligned} \right\} \quad (2)$$

where

$$\begin{aligned}
\tilde{\rho} &\ll 1 & \tilde{u} &\ll 1 & \tilde{v} &\ll 1 & \tilde{\mu} &\ll 1 & \tilde{p} &\ll (\gamma M_0^2)^{-1} \\
\tilde{\varepsilon} &\ll [(\gamma - 1)\gamma M_0^2]^{-1}
\end{aligned}$$

Here, $M_0 = u_0(\gamma p_0/\rho_0)^{-1/2}$ is the Mach number at infinity, which is always assumed to be less than unity. By substituting expressions (2) into equations (1) and retaining only the first-order terms with respect to small perturbations \tilde{u} , \tilde{v} , \tilde{p} , $\tilde{\rho}$, $\tilde{\varepsilon}$, and $\tilde{\mu}$, we obtain the following system of linear partial differential equations with constant coefficients:

$$\mathbf{C} \frac{\partial \mathbf{u}}{\partial t} + \mathbf{D} \frac{\partial \mathbf{u}}{\partial x} + \mathbf{F} \frac{\partial \mathbf{u}}{\partial y} + \mathbf{H} \frac{\partial^2 \mathbf{u}}{\partial y^2} = \mathbf{0} \quad (3a)$$

where

$$\left. \begin{aligned} \mathbf{u} &= \begin{bmatrix} u \\ v \\ p \\ \rho \end{bmatrix} & \mathbf{C} &= \begin{bmatrix} 0 & 0 & 0 & 1 \\ 1 & 0 & 0 & 0 \\ 0 & 1 & 0 & 0 \\ 0 & 0 & 1 & -M_0^{-2} \end{bmatrix} & \mathbf{D} &= \begin{bmatrix} 1 & 0 & 0 & 1 \\ 1 & 0 & 1 & 0 \\ 0 & 1 & 0 & 0 \\ 0 & 0 & 1 & -M_0^{-2} \end{bmatrix} \\ \mathbf{F} &= \begin{bmatrix} 0 & 1 & 0 & 0 \\ 0 & 0 & 0 & 0 \\ 0 & 0 & 1 & 0 \\ 0 & 0 & 0 & 0 \end{bmatrix} & \mathbf{H} &= -\frac{1}{Re} \begin{bmatrix} 0 & 0 & 0 & 0 \\ 1 & 0 & 0 & 0 \\ 0 & 4/3 & 0 & 0 \\ 0 & 0 & \gamma Pr^{-1} & -Pr^{-1} M_0^{-2} \end{bmatrix} \end{aligned} \right\} \quad (3b)$$

The system (3) is the linearization of equations (1) against the free-stream background. We omit the tilde in equations (3) since we are going to deal only with linear equations in perturbations henceforth.

Additionally, we used the equation of state $\varepsilon = \frac{1}{\gamma - 1} \frac{p}{\rho}$ (more precisely, its linearization $\tilde{\varepsilon} = \frac{1}{\gamma - 1} \left(\tilde{p} - \frac{1}{\gamma M_0^2} \tilde{\rho} \right)$) to eliminate internal energy from equations (3).

We have mentioned that equations (3) will be used for the description of fluid motion in the far field. Let us now define a general geometric setup for the problem under consideration. The original Navier-Stokes equations are integrated on a grid (e.g., *C*-type) generated around the airfoil; this grid covers the finite computational domain which is denoted D_{in} hereafter. (See fig. 1.) We henceforth assume that the linearization (eqs. (3)) is valid outside the computational domain D_{in} , i.e., on its complement D_{ex} . (See fig. 1.) This assumption is true for large computational domains, i.e., far enough from the immersed body. As we approach the airfoil, the possibility of linearization in D_{ex} can always be verified *a posteriori* by analyzing the corresponding computational results (as was done in refs. 11 and 12 for the steady-state case).

To integrate the Navier-Stokes equations on the grid inside D_{in} , we use some finite-dimensional approximation of these equations. The actual type of the resulting discrete operator (i.e., finite-difference, finite-element, etc.) is not that important from the standpoint of constructing the ABC's; for definiteness we assume that the Navier-Stokes equations are integrated by means of a finite-difference scheme. To begin with, we also suppose that this scheme is fully explicit in time. We may think that we already know the solution for the time level t^l on the entire grid, in particular, $l = 0$ implies the initial data. When we advance one time step, i.e., calculate the solution for the level t^{l+1} by means of the scheme, we cannot obtain this solution for the whole grid since some nodes located near the external boundary of D_{in} will be missing. The actual location of missing nodes depends on the specific structure of the scheme stencil. For example, a typical central-difference second-order approximation to the spatial part of the Navier-Stokes operator on a structured grid requires a 3×3 stencil. Using such a spatial approximation combined with an explicit integration procedure in time, we can obtain the solution on the level t^{l+1} at all nodes, except for those that belong to the outermost coordinate row of the grid (designated Γ_1 in fig. 1). To advance the next time step (t^{l+2}) we will have to somehow determine these missing values of the solution on the level t^{l+1} . This will be done by means of solving the linearized system in D_{ex} (i.e., by representing its solution in the form of the generalized potential for each Fourier

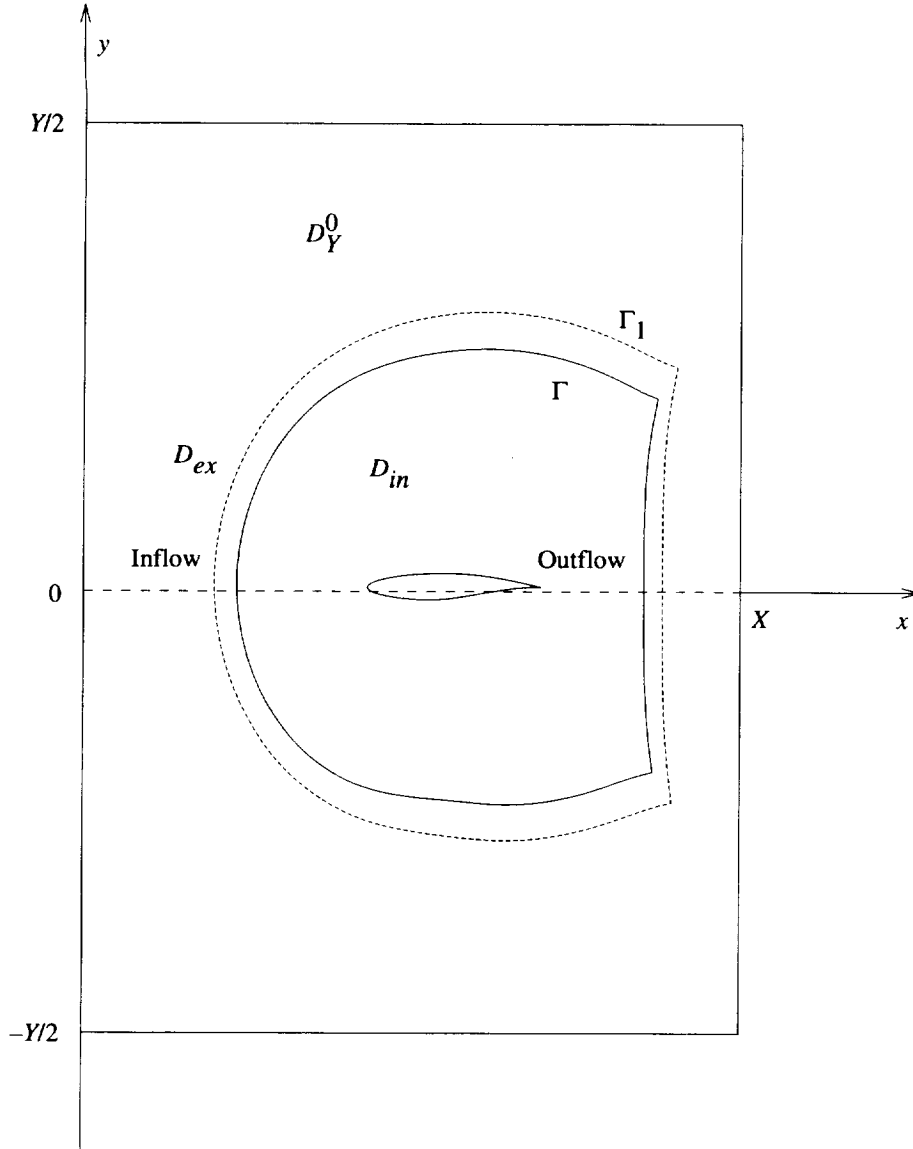


Figure 1. Configuration of domains.

mode). In other words, using the solution to equations (3) in D_{ex} we close the system of difference equations inside the computational domain D_{in} . The closure we obtain is actually the desirable ABC's.

Note that in the case of steady-state problems the ABC's (ref. 8) were also used to close the subdefinite system of difference equations inside D_{in} . As previously mentioned, boundary conditions (ref. 8) were implemented in references 11 and 12 together with the pseudo-time iteration procedure for achieving the steady state. (See refs. 13–15.) From an algorithmic standpoint, this approach is almost the same as the true integration in time, so the ABC's (ref. 8) were applied on the upper time level for each iteration. However, there is an essential difference between the approach in reference 8 and the technique to be described in this paper. Namely, the former is intended only for the treatment of steady-state problems and is based on the linearized stationary equations, and the latter will take into account the previous evolution of the solution in time.

Additionally, let us note that in the case of implicit schemes we also need ABC's that will complete the system of difference equations inside D_{in} . Indeed, while integrating the Navier-Stokes equations by

means of an implicit scheme one has to solve a certain discrete system on the upper time level (t^{l+1}), whereas the data from the lower time level(s) play the role of forcing terms. This system will obviously be subdefinite unless we specify additional relations that connect the values of unknowns in the grid nodes located near the external boundary. In particular, for the previously-mentioned example of a structured grid and central differences on the 3×3 spatial stencil, these additional relations (i.e., the ABC's) should connect the values of the solution at the penultimate (the curve Γ in fig. 1) and outermost rows of grid nodes. (See also refs. 8, 11, and 12.) Including the missing relations provided by the ABC's into the system solved on the upper time level, we close this system and then advance the next time step.

Let us now provide an exact formulation of the problem. First, we select those nodes of the grid where the solution can no longer be determined by the scheme but must be obtained by means of special additional relations (i.e., by means of the ABC's). We designate this set of nodes v_1 . Second, we select those nodes of the grid where we need to know the solution in order to obtain it on v_1 with the help of the ABC's. The latter set is designated v . Both v and v_1 will depend on the structure of the specific stencil. In particular, for the 3×3 stencil on a structured grid, v and v_1 correspond to the penultimate and outermost rows of grid nodes, respectively. (Also see refs. 8, 11, and 12.) Without loss of generality, we assume that the artificial boundary Γ (see fig. 1) is formed by the penultimate row of nodes v , so that all nodes v_1 that form the curve Γ_1 (see fig. 1) already belong to D_{ex} (i.e., to the "linear zone").

Then, we designate the time period by T . Clearly, we can further consider our problem for the time interval $[0, T]$ without loss of generality. We will also need the following brief notations: $D_{ex}^T = D_{ex} \times [0, T]$, $D_{in}^T = D_{in} \times [0, T]$, $\Gamma^T = \Gamma \times [0, T]$, and $\Gamma_1^T = \Gamma_1 \times [0, T]$. The closure of the finite-difference system in D_{in}^T , which we are looking for and which should be provided by the ABC's, is actually a set of relations expressing $\mathbf{u}|_{\Gamma_1^T}$ in terms of some data specified on Γ^T . As previously mentioned, these relations will be based on the solution to the linearized system (3) in D_{ex}^T . The latter system is supplemented (on D_{ex}^T) by the periodicity condition in time,

$$\mathbf{u}|_{t=0} = \mathbf{u}|_{t=T} \quad ((x, y) \in D_{ex}) \quad (4)$$

and the free-stream condition at infinity,

$$\mathbf{u} \rightarrow \mathbf{0} \text{ as } x^2 + y^2 \rightarrow \infty \quad (t \in [0, T]) \quad (5)$$

The choice of the data on Γ^T that "drive" the ABC's is closely connected to the concept of *clear trace*, delineated in references 9 and 10. The question of the possible proper constructions of clear traces for equations (3) may require a special thorough investigation in addition to the general analysis from references 9 and 10; such an investigation is not a direct subject of this paper. Therefore, we will not comment on this question in our further discussion, we only point out the actual construction we use. Namely, let us first represent the vector function $\mathbf{u}(x, y, t)$ in the form of a Fourier series in time for any space point (x, y) ,

$$\mathbf{u}(x, y, t) = \sum_{n=-\infty}^{n=\infty} \hat{\mathbf{u}}^n(x, y) e^{int \frac{2\pi}{T}} \quad (6)$$

where

$$\hat{\mathbf{u}}^n(x, y) = \frac{1}{T} \int_0^T \mathbf{u}(x, y, t) e^{-int \frac{2\pi}{T}} dt \quad (n = 0, \pm 1, \pm 2, \dots) \quad (7)$$

Instead of considering equations (3a), (4), and (5) D_{ex}^T , we henceforth consider D_{ex} the family of “stationary” systems,

$$i\omega_n \mathbf{C}\hat{\mathbf{u}}^n + \mathbf{D}\frac{\partial \hat{\mathbf{u}}^n}{\partial x} + \mathbf{F}\frac{\partial \hat{\mathbf{u}}^n}{\partial y} + \mathbf{H}\frac{\partial^2 \hat{\mathbf{u}}^n}{\partial y^2} = \mathbf{0} \quad (n = 0, \pm 1, \pm 2, \dots) \quad (8)$$

parameterized by the frequency $\omega_n = 2\pi n/T$, $n = 0, \pm 1, \pm 2, \dots$, and supplemented at infinity by the boundary conditions

$$\hat{\mathbf{u}}^n(x, y) \rightarrow \mathbf{0} \text{ as } x^2 + y^2 \rightarrow \infty \quad (n = 0, \pm 1, \pm 2, \dots) \quad (9)$$

which directly follow from formula (5). The matrices \mathbf{C} , \mathbf{D} , \mathbf{F} , and \mathbf{H} in the system (8) are the same as in formula (3b).

For each frequency ω_n we consider the pair of functions $\left(\hat{\mathbf{u}}_\Gamma^n, \frac{\partial \hat{\mathbf{u}}_\Gamma^n}{\partial \zeta}\right)$ (specified on Γ) as the data that “drive” the ABC’s; here, ζ is the normal to Γ . (Note that if the interior solution is already computed by means of the scheme inside D_{in}^T , then $\hat{\mathbf{u}}_\Gamma^n$ and $\frac{\partial \hat{\mathbf{u}}_\Gamma^n}{\partial \zeta}$ can be easily calculated.)

Our ultimate goal will be to provide a full classification of those and only those functions $\left(\hat{\mathbf{v}}_\Gamma^n, \frac{\partial \hat{\mathbf{v}}_\Gamma^n}{\partial \zeta}\right)$ (defined on Γ) that generate a solution $\hat{\mathbf{u}}^n(x, y)$ to system (8) (with boundary conditions (9) defined on D_{ex} and such that its trace on Γ coincides with the “source” function itself, i.e.,

$$\left(\hat{\mathbf{u}}^n, \frac{\partial \hat{\mathbf{u}}^n}{\partial \zeta}\right)\Big|_\Gamma = \left(\hat{\mathbf{v}}_\Gamma^n, \frac{\partial \hat{\mathbf{v}}_\Gamma^n}{\partial \zeta}\right) \quad (10)$$

As will be seen from further consideration, the corresponding set of functions $\left(\hat{\mathbf{v}}_\Gamma^n, \frac{\partial \hat{\mathbf{v}}_\Gamma^n}{\partial \zeta}\right)$ can be described as an image of a certain boundary projection operator. In other words, the functions $\left(\hat{\mathbf{v}}_\Gamma^n, \frac{\partial \hat{\mathbf{v}}_\Gamma^n}{\partial \zeta}\right)$ will satisfy some boundary operator equation with projection. (The equation of this type was mentioned in the introduction as the one equivalent to the linearized exterior problem.) Let us designate the corresponding projection operator by \mathbf{P}_Γ^n (we actually construct this operator in section 3). Then, specifying any function $\left(\hat{\mathbf{u}}_\Gamma^n, \frac{\partial \hat{\mathbf{u}}_\Gamma^n}{\partial \zeta}\right)$ (from inside D_{in}), we apply \mathbf{P}_Γ^n and consider the projection $\mathbf{P}_\Gamma^n\left(\hat{\mathbf{u}}_\Gamma^n, \frac{\partial \hat{\mathbf{u}}_\Gamma^n}{\partial \zeta}\right) = \left(\hat{\mathbf{v}}_\Gamma^n, \frac{\partial \hat{\mathbf{v}}_\Gamma^n}{\partial \zeta}\right)$ as the right-hand side in equality (10) for the problem (eqs. (8)–(10)). After solving the problem (eqs. (8)–(10)) on D_{ex} , we find the trace of its solution on Γ_1 (i.e., on \mathbf{v}_1), which in turn enables us to obtain the missing boundary relations that close the system of difference equations inside D_{in}^T . These relations (i.e., the ABC’s) are derived using the inverse Fourier transform. They can be symbolically written as

$$\mathbf{u}_{v_1} = \left[\mathbf{P}_{ex}^n \circ \mathbf{P}_{\Gamma}^n \circ \mathbf{R} \left(\hat{\mathbf{u}}_v^n, \frac{\partial \hat{\mathbf{u}}_v^n}{\partial \zeta} \right) \right] \Big|_{v_1} \quad (t \in [0, T]) \quad (11)$$

where the operator \mathbf{R} represents some (smooth) interpolation of the discrete functions along the curve Γ , and the operator \mathbf{P}_{ex}^n involves the calculation of the generalized potential to solve the problem (eqs. (8)–(10)). The specific structure of all operators from formula (11) will be delineated in section 3, where we actually construct their discrete counterparts.

Let us make a few important remarks. First, to formally close the system solved in D_{in}^T , we have to obtain additional relations between the values of the unknowns on Γ^T and on Γ_1^T . Such relations would provide ABC's that are completely independent of any specific numerical procedure employed inside D_{in}^T . However, to simplify our task and at the same time only slightly compromise the previously-mentioned independence, we take into account that we almost always integrate the Navier-Stokes equations step-by-step in time (explicitly or implicitly). Therefore, we do not have to construct such ABC's that would connect the values of the solution at v and at v_1 for all time moments $t \in [0, T]$. It suffices to determine u , v , p , and ρ at v_1 only for $t = T$ (i.e., at the upper time level) since for all previous moments these values have been determined when calculating previous time steps. Moreover, the formulation of the problem (eqs. (8)–(10)), where the right-hand side from equality (10) belongs to the projection image, $\left(\hat{\mathbf{v}}_{\Gamma}^n, \frac{\partial \hat{\mathbf{v}}_{\Gamma}^n}{\partial \zeta} \right) \in \text{Im } \mathbf{P}_{\Gamma}^n$, assumes that these data are a result of operating by \mathbf{P}_{Γ}^n on the Fourier transform $\left(\hat{\mathbf{u}}_{\Gamma}^n, \frac{\partial \hat{\mathbf{u}}_{\Gamma}^n}{\partial \zeta} \right)$ of some time-periodic function. However, in conducting the step-by-step integration in time, the actual data $\left(\mathbf{u}_{\Gamma}, \frac{\partial \mathbf{u}_{\Gamma}}{\partial \zeta} \right)$ may not be periodic until we achieve a true oscillatory regime. Therefore, as mentioned in the introduction, any time we use the ABC's we implement a certain generalized treatment of the external flow as being already time-periodic. Namely, instead of the true boundary data $\left(\mathbf{u}_{\Gamma}, \frac{\partial \mathbf{u}_{\Gamma}}{\partial \zeta} \right)$ at Γ^T , we use the best approximation of this data by periodic functions in the sense of least squares. This approach will be delineated in section 3, which is devoted to numerics.

Second, we are unable to directly solve the problem (eqs. (8)–(10)) on D_{ex} since the domain is infinite. Handling of this problem will require the additional truncation. Recall that we have already truncated the original infinite domain and have obtained D_{in} ; now we also truncate D_{ex} in order to get a new linear problem formulated on a finite domain, and therefore, available for solution on the computer. This issue is addressed in subsection 2.3.

Third, we certainly will not solve the problem (eqs. (8)–(10)) every time we need to obtain a closed system inside D_{in} (i.e., each time step). Instead, using the linearity of the problem, we will specify some basis in the space of boundary data and solve the problem (eqs. (8)–(10)) one time for each basis function. This approach will enable us to obtain the ABC's in matrix form, which is very convenient for practical computing. (Also see refs. 8, 11, and 12.)

Ultimately we will deal only with the finite-difference formulations and, consequently, with the finite Fourier series (instead of the infinite series (6), see section 3). In so doing, the discretization in time for the linearized exterior problem in D_{ex}^T should not necessarily coincide with the one used for the Navier-Stokes scheme inside D_{in}^T . A more convenient method may be to use interpolation in time, which was previously proposed in reference 16.

Finally, let us mention that since we need to know the solution on Γ for the whole period T to restore the solution on v_1 , the first few time steps (until the total time reaches T) will require some special treatment. It might be based on the usage of either a larger grid or some other external boundary conditions for the initial stage of integration in time.

We now proceed to the actual construction of the operators involved in formula (11). This construction will be essentially the same for all wavenumbers n (n is contained as a parameter in the corresponding expressions hereafter).

As was mentioned before, the computation of the ABC's (eq. (11)) consists of two stages. First we apply the projection \mathbf{P}_Γ^n to provide the proper boundary data (right-hand side of equality (10) for the problem (eqs. (8)–(10)). Then we find the solution to the problem (eqs. (8)–(10)) in the form of the generalized potential (operator \mathbf{P}_{ex}^n). Both of these stages will require the application of the DPM. (See refs. 9 and 10.) In particular, it appears that the computation of \mathbf{P}_Γ^n and \mathbf{P}_{ex}^n requires the solution of the same *auxiliary problem* (AP) described in sections 2.2 and 2.3 for the continuous formulation and in section 3.2 for the difference formulation. This AP is actually the main element of the DPM-based approach. The Green operator of the AP plays in the theory of generalized potentials approximately the same role as the Green function (or the fundamental solution) plays in classical potential theory. (See refs. 9 and 10.) The AP is formulated on the entire plane (x, y) for the inhomogeneous counterpart of system (8) with a certain compactly supported right-hand side $\hat{\mathbf{f}}^n = (\hat{f}_1^n, \hat{f}_2^n, \hat{f}_3^n, \hat{f}_4^n)$ (to be specified later on). Namely, we will need to solve the following system,

$$i\omega_n \mathbf{C}\hat{\mathbf{u}}^n + \mathbf{D}\frac{\partial \hat{\mathbf{u}}^n}{\partial x} + \mathbf{F}\frac{\partial \hat{\mathbf{u}}^n}{\partial y} + \mathbf{H}\frac{\partial^2 \hat{\mathbf{u}}^n}{\partial y^2} = \hat{\mathbf{f}}^n \quad (12)$$

on R^2 , $\text{supp}\hat{\mathbf{f}}^n(x, y) \subset D_{in}$, and we will require that the solution be unique in the class of functions vanishing at infinity. In other words, system (12) is supplemented by the following boundary condition,

$$\hat{\mathbf{u}}^n(x, y) \rightarrow \mathbf{0} \text{ as } x^2 + y^2 \rightarrow \infty \quad (13)$$

which is the same as boundary conditions (9).

Once we are able to solve the AP (eqs. (12) and (13)), we can construct the boundary operator \mathbf{P}_Γ^n , properly formulate the problem (eqs. (8)–(10)), and finally obtain its solution in the form of a generalized potential. This is actually a very brief description of our DPM-based approach; it will be delineated in section 3 for the discrete formulation of the problem. Now we will investigate the solvability of the AP (eqs. (12) and (13)).

2.2. Solvability of Linearized Problem on Entire Plane

We will look for the solution to the AP (eqs. (12) and (13)) in the space of tempered distributions \mathcal{G}' (see ref. 19 by Hörmander or ref. 20 by Vladimirov), which is a conjugate space to the space \mathcal{G} of all infinitely smooth functions defined on R^2 that decrease at infinity with all their derivatives faster than any power of $(x^2 + y^2)^{-1/2}$. Take the Fourier transform

$$\hat{\hat{\mathbf{u}}}^n(\xi, \eta) = \frac{1}{2\pi} \int_{-\infty}^{\infty} \int_{-\infty}^{\infty} \hat{\mathbf{u}}^n(x, y) e^{-i\xi x - i\eta y} dx dy \quad (14a)$$

$$\hat{\hat{\mathbf{f}}}^n(\xi, \eta) = \frac{1}{2\pi} \int_{-\infty}^{\infty} \int_{-\infty}^{\infty} \hat{\mathbf{f}}^n(x, y) e^{-i\xi x - i\eta y} dx dy \quad (14b)$$

of both sides of system (12) and represent the result in the form of a matrix equation,

$$\mathbf{Q}\hat{\mathbf{u}} = \hat{\mathbf{f}} \quad (15)$$

Note that in system (15) and henceforth in this subsection we drop the superscript n to simplify the notations. Then, the symbol \mathbf{Q} (eq. (15)) is given by

$$\mathbf{Q} = i\omega\mathbf{C} + i\xi\mathbf{D} + i\eta\mathbf{F} - \eta^2\mathbf{H}$$

$$= \begin{bmatrix} i\xi & i\eta & 0 & i(\omega + \xi) \\ i(\omega + \xi) + \frac{\eta^2}{Re} & 0 & i\xi & 0 \\ 0 & i(\omega + \xi) + \frac{4}{3}\frac{\eta^2}{Re} & i\eta & 0 \\ 0 & 0 & i(\omega + \xi) + \frac{\gamma\eta^2}{RePr} & -\frac{i}{M_0^2}(\omega + \xi) - \frac{\eta^2}{RePrM_0^2} \end{bmatrix} \quad (16)$$

We first show that system (15) is solvable in \mathcal{G}' . For the time being, we do not need any restrictive assumptions in regard to $\hat{\mathbf{f}}$; as previously mentioned, $\hat{\mathbf{f}}$ is compactly supported ($\text{supp}\hat{\mathbf{f}} \subset D_{in}$), and without loss of generality we may think that $\hat{\mathbf{f}}$ is absolutely integrable on R^2 ($\hat{\mathbf{f}} \in L^1(R^2)$). Then, its Fourier transform $\hat{\hat{\mathbf{f}}}$ is bounded and continuous on R^2 ; consequently, if we formally write down the solution to system (15) as

$$\hat{\mathbf{u}} = \mathbf{Q}^{-1}\hat{\hat{\mathbf{f}}} \quad (17)$$

then the properties of the right-hand side in equality (17) are fully determined by the inverse symbol \mathbf{Q}^{-1} . Indeed, it is well known (ref. 20) that if the right-hand side of equality (17) is locally absolutely integrable on R^2 then it defines the tempered distribution, i.e., the generalized function from \mathcal{G}' . The latter will coincide (in the sense of distributions) with the classical function $\mathbf{Q}^{-1}(\xi, \eta)\hat{\hat{\mathbf{f}}}(\xi, \eta)$ everywhere on R^2 , except for the set of singularities of $\mathbf{Q}^{-1}(\xi, \eta)\hat{\hat{\mathbf{f}}}(\xi, \eta)$ (if any). Since in our case the function $\hat{\hat{\mathbf{f}}}(\xi, \eta)$ is continuous and bounded on R^2 , then it suffices to determine whether the function $\mathbf{Q}^{-1}(\xi, \eta)$ belongs to $L^1_{\text{loc}}(R^2)$.

To do this, we have to find all singularities of $\mathbf{Q}^{-1}(\xi, \eta)$. Calculating the determinant of $\mathbf{Q}(\xi, \eta)$, we obtain

$$Q(\xi, \eta) = \left[-(\omega + \xi)^4 + \frac{(\omega + \xi)^2}{M_0^2}(\xi^2 + \eta^2) + \frac{(\omega + \xi)^2\eta^4}{Re^2}\left(\frac{4}{3} + \frac{7}{3}\frac{\gamma}{Pr}\right) - \frac{4}{3}\frac{\xi^2\eta^4}{M_0^2PrRe^2} - \frac{\eta^6}{M_0^2PrRe^2} \right]$$

$$+ i \left[\frac{(\omega + \xi)^3\eta^2}{Re}\left(\frac{7}{3} + \frac{\gamma}{Pr}\right) - \frac{(\omega + \xi)\xi^2\eta^2}{M_0^2Re}\left(\frac{4}{3} + \frac{1}{Pr}\right) - \frac{(\omega + \xi)\eta^4}{M_0^2Re}\left(1 + \frac{1}{Pr}\right) - \frac{4}{3}\frac{(\omega + \xi)\eta^6}{PrRe^3} \right] \quad (18)$$

Here ξ and η are the variables and ω , M_0 , Re , Pr , and γ are parameters. We emphasize that both variables ξ and η are supposed to be real (see formulas (14)); however, the coefficients of $Q(\xi, \eta)$ are, generally speaking, complex. Thus, to find singular points of the symbol \mathbf{Q} (eq. (16)), one has to find the real roots of $Q(\xi, \eta)$ (eq. (18)), which actually implies to find common real roots of two polynomials, $\Re Q(\xi, \eta)$ and $\Im Q(\xi, \eta)$. First, the point ($\xi = -\omega$, $\eta = 0$) is clearly one of such common roots. Then, we

note that $\Im Q(\xi, \eta)$ turns into zero on the two entire straight lines, $\xi = -\omega$ and $\eta = 0$. Moreover, $\Re Q(\xi, \eta)$ has no other roots on the line $\xi = -\omega$, except for $\eta = 0$. Further, substituting $\eta = 0$ into the equation $\Re Q(\xi, \eta) = 0$ (see formula (18)) and assuming that $\xi \neq -\omega$, we find the following two roots of

$\Re Q(\xi, \eta) = 0$ that belong to the line $\eta = 0$: $\xi_1 = \frac{\omega M_0}{1 - M_0}$ and $\xi_2 = -\frac{\omega M_0}{1 + M_0}$. We also observe that if

$\omega = 0$ (which corresponds to the steady-state flows), then all three roots, $(-\omega, 0)$, $\left(\frac{\omega M_0}{1 - M_0}, 0\right)$, and

$\left(-\frac{\omega M_0}{1 + M_0}, 0\right)$, merge into one.

In an attempt to find other real roots (if any) of $Q(\xi, \eta)$ (eq. (18)), we divide the equation $\Im Q(\xi, \eta) = 0$ by $(\omega + \xi)\eta^2/Re$. (This is possible since we have already proven that no other zeros exist on the two lines $\xi = -\omega$ and $\eta = 0$, except for those already found.) The resulting equation,

$$(\omega + \xi)^2 \left(\frac{7}{3} + \frac{\gamma}{Pr} \right) - \frac{\xi^2}{M_0^2} \left(\frac{4}{3} + \frac{1}{Pr} \right) - \frac{\eta^2}{M_0^2} \left(1 + \frac{1}{Pr} \right) - \frac{4}{3} \gamma \frac{\eta^4}{Pr Re^2} = 0 \quad (19)$$

is of fourth order, and taking into account that the equation $\Re Q(\xi, \eta) = 0$ (see formula (18)) is of sixth order, we conclude that the polynomial $Q(\xi, \eta)$ may have not more than a finite number of isolated real roots in total (three of which have already been found). We emphasize here that this property (finite number of isolated real roots) presents an essential difference between the problem under investigation and classical acoustics problems in which the viscous terms in the governing equations are usually neglected. Namely, for the acoustics equations (i.e., linearized Euler equations) the singular points of the symbol are no longer isolated. They usually form a curve on the plane R^2 which may cause noticeable difficulties with justification of the uniqueness of solution. These difficulties are similar to those that arise in studying the Helmholtz equation, which may be referred to as describing acoustics in the stationary medium. We do not deal with Helmholtz-like equations in this paper; we only note that contrary to the acoustics case, system (12) is presumably easier from this standpoint since the proof of uniqueness appears to be elementary. (See proposition 4.)

Since equation (19) is of second order with respect to ξ we can resolve it for each η and obtain explicit function(s) $\xi_3 = \xi_3(\eta)$. Because we are interested only in real solutions, we have to consider a few different cases.

First, assume that $\omega \neq 0$. Then, rewrite equation (19) as

$$\xi^2 \left[\frac{7}{3} + \frac{\gamma}{Pr} - \frac{1}{M_0^2} \left(\frac{4}{3} + \frac{1}{Pr} \right) \right] + 2\omega\xi \left(\frac{7}{3} + \frac{\gamma}{Pr} \right) + \omega^2 \left(\frac{7}{3} + \frac{\gamma}{Pr} \right) - \frac{\eta^2}{M_0^2} \left(1 + \frac{1}{Pr} \right) - \frac{4}{3} \gamma \frac{\eta^4}{Pr Re^2} = 0 \quad (20)$$

and observe that, if $M_0^2 = \left(\frac{4}{3} + \frac{1}{Pr} \right) \left(\frac{7}{3} + \frac{\gamma}{Pr} \right)^{-1}$, then equation (20) degenerates and therefore has a

unique real solution $\xi_3^{(0)} = \xi_3^{(0)}(\eta)$ for any η . If $M_0^2 > \left(\frac{4}{3} + \frac{1}{Pr} \right) \left(\frac{7}{3} + \frac{\gamma}{Pr} \right)^{-1}$, then we can easily make sure that the discriminant

$$D = 4\omega^2 \left(\frac{7}{3} + \frac{\gamma}{Pr} \right)^2 - 4 \left[\frac{7}{3} + \frac{\gamma}{Pr} - \frac{1}{M_0^2} \left(\frac{4}{3} + \frac{1}{Pr} \right) \right] \left[\omega^2 \left(\frac{7}{3} + \frac{\gamma}{Pr} \right) - \frac{\eta^2}{M_0^2} \left(1 + \frac{1}{Pr} \right) - \frac{4}{3} \gamma \frac{\eta^4}{Pr Re^2} \right] \quad (21)$$

is always positive, which means that equation (19) has two different real solutions, $\xi_3^{(1)} = \xi_3^{(1)}(\eta)$ and $\xi_3^{(2)} = \xi_3^{(2)}(\eta)$ for any η . If $M_0^2 < \left(\frac{4}{3} + \frac{1}{Pr}\right)\left(\frac{7}{3} + \frac{\gamma}{Pr}\right)^{-1}$, then the condition $D \geq 0$ (see formula (21)) imposes certain restrictions on η . Namely, we have

$$-\left(\frac{3PrRe^2}{8\gamma}\left[-\frac{1}{M_0^2}\left(1 + \frac{1}{Pr}\right) + \sqrt{D_1}\right]\right)^{1/2} \leq \eta \leq \left(\frac{3PrRe^2}{8\gamma}\left[-\frac{1}{M_0^2}\left(1 + \frac{1}{Pr}\right) + \sqrt{D_1}\right]\right)^{1/2} \quad (22)$$

where

$$D_1 = \frac{1}{M_0^4}\left(1 + \frac{1}{Pr}\right)^2 - \frac{16}{3} \frac{\gamma\omega^2}{PrRe^2M_0^2}\left(\frac{7}{3} + \frac{\gamma}{Pr}\right)\left(\frac{4}{3} + \frac{1}{Pr}\right)\left[\frac{7}{3} + \frac{\gamma}{Pr} - \frac{1}{M_0^2}\left(\frac{4}{3} + \frac{1}{Pr}\right)\right]^{-1}$$

Therefore, in this case the real solutions to equation (19), $\xi_3^{(1)} = \xi_3^{(1)}(\eta)$ and $\xi_3^{(2)} = \xi_3^{(2)}(\eta)$, exist only for η within the above range. (See inequality (22)).

Now consider the case $\omega = 0$ (which corresponds to the steady-state problem). From equation (19), we easily derive

$$\xi^2\left[\frac{7}{3} + \frac{\gamma}{Pr} - \frac{1}{M_0^2}\left(\frac{4}{3} + \frac{1}{Pr}\right)\right] = \frac{\eta^2}{M_0^2}\left(1 + \frac{1}{Pr}\right) + \frac{4}{3}\gamma\frac{\eta^4}{PrRe^2} \quad (23)$$

Equation (23) has real solutions, $\xi_3^{(1)} = \xi_3^{(1)}(\eta)$ and $\xi_3^{(2)} = \xi_3^{(2)}(\eta)$, only for $M_0^2 > \left(\frac{4}{3} + \frac{1}{Pr}\right)\left(\frac{7}{3} + \frac{\gamma}{Pr}\right)^{-1}$. Otherwise, we conclude that the equation $\Im Q(\xi, \eta) = 0$ for $\omega = 0$ has no other real roots except for $(\xi = 0, \eta = 0)$ and therefore, the same is true for the equation $Q(\xi, \eta) = 0$.

In practice, we have calculated explicit symbolic expressions for the functions $\xi_3^{(0)} = \xi_3^{(0)}(\eta)$, $\xi_3^{(1)} = \xi_3^{(1)}(\eta)$, and $\xi_3^{(2)} = \xi_3^{(2)}(\eta)$ using *Mathematica*. (See ref. 21 by Wolfram.) (These expressions are not presented here because they are fairly cumbersome.) Then, substituting the functions $\xi_3^{(0)} = \xi_3^{(0)}(\eta)$, $\xi_3^{(1)} = \xi_3^{(1)}(\eta)$, and $\xi_3^{(2)} = \xi_3^{(2)}(\eta)$ into the second equation, $\Re Q(\xi, \eta) = 0$, we obtain the algebraic equations with respect to only one variable η . Clearly the above equations (which are different for the different solutions, $\xi_3^{(0)} = \xi_3^{(0)}(\eta)$, $\xi_3^{(1)} = \xi_3^{(1)}(\eta)$, and $\xi_3^{(2)} = \xi_3^{(2)}(\eta)$) may have real root(s) if and only if the original equation $Q(\xi, \eta) = 0$ has other real zero(s) besides those that have already been found, $(-\omega, 0)$, $\left(\frac{\omega M_0}{1 - M_0}, 0\right)$, and $\left(-\frac{\omega M_0}{1 + M_0}, 0\right)$. Therefore, we finally have reduced the question about the real zeros of the equation $Q(\xi, \eta) = 0$ to the question about the real root(s) of certain algebraic equations of one variable.

Regrettably, the resulting equations (after the substitution of $\xi_3^{(0)} = \xi_3^{(0)}(\eta)$, $\xi_3^{(1)} = \xi_3^{(1)}(\eta)$, and $\xi_3^{(2)} = \xi_3^{(2)}(\eta)$ into $\Re Q(\xi, \eta) = 0$) appear to be too complicated for obtaining general expressions for their real root(s). However, we may implement the following semi-numerical approach which provides fairly convincing results.

First, note that the case $\omega = 0$ seems to be the simplest one. This case actually admits rigorous analysis without doing any simplifying assumptions. As previously mentioned, equation (23) has no real

solutions for $M_0^2 < \left(\frac{4}{3} + \frac{1}{Pr}\right)\left(\frac{7}{3} + \frac{\gamma}{Pr}\right)^{-1}$ (which implies that the determinant (eq. (18)) has no real roots); for $M_0^2 = \left(\frac{4}{3} + \frac{1}{Pr}\right)\left(\frac{7}{3} + \frac{\gamma}{Pr}\right)^{-1}$ equation (23) degenerates and any pair (ξ, η) of the kind ξ is arbitrary, $\eta = 0$ is its root. Substituting this root into $\Re Q(\xi, \eta) = 0$ (see eq. (18)), we obtain $\xi^4(1/M_0^2 - 1) = 0$, which yields $\xi = 0$. Therefore, we did not find any new real zero. For $M_0^2 > \left(\frac{4}{3} + \frac{1}{Pr}\right)\left(\frac{7}{3} + \frac{\gamma}{Pr}\right)^{-1}$, equation (23) has two different real solutions for any η ; moreover, $\xi_3^{(1)} = \xi_3^{(1)}(\eta) = -\xi_3^{(2)} = -\xi_3^{(2)}(\eta)$. Since all powers of ξ in $\Re Q(\xi, \eta)$ are even, we do not need to separately consider $\xi_3^{(1)} = \xi_3^{(1)}(\eta)$ and $\xi_3^{(2)} = \xi_3^{(2)}(\eta)$. Substituting $\xi_3^{(1,2)} = \xi_3^{(1,2)}(\eta)$ into $\Re Q(\xi, \eta) = 0$, we obtain the following eighth-order equation with respect to η : $a\eta^8 + b\eta^6 + c\eta^4 = 0$, where the coefficients a , b , and c are obviously real. The explicit expressions for a , b , and c were obtained by means of *Mathematica* (see ref. 21); we do not present them here because they are cumbersome. However, using these expressions we can prove that $a > 0$, $b > 0$, and $c > 0$. Then, it becomes clear that there are no other real roots except for the one we have already found, $\eta = 0$ (which also yields $\xi = 0$). Indeed, the equation $a\eta^4 + b\eta^2 + c = 0$ for $a > 0$, $b > 0$, and $c > 0$ may have only essentially complex roots η . Therefore, we conclude that for $\omega = 0$ the symbol \mathbf{Q} (eq. (16)) has only one singular point ($\xi = 0, \eta = 0$).

Recall that all equations under study generally depend on five real parameters, ω, M_0, Re, Pr , and γ . To simplify our task, we fix the values of some of these parameters. Let us set $\gamma = 1.4$ (two-atom gas) and $Pr = 0.72$ (air). This choice of values for the ratio of specific heats and for the Prandtl number, respectively, is most frequently used since it is closely related to numerous practical problems; we will not consider any other numerical values for these two parameters. We now investigate another simple case, $\omega \neq 0$, $M_0^2 = \left(\frac{4}{3} + \frac{1}{Pr}\right)\left(\frac{7}{3} + \frac{\gamma}{Pr}\right)^{-1}$. Then, we have

$$\xi_3^{(0)}(\eta) = -\frac{\omega}{2} + \left[\frac{\eta^2}{M_0^2} \left(1 + \frac{1}{Pr}\right) + \frac{4}{3} \gamma \frac{\eta^4}{Pr Re^2} \right] \left[\left(\frac{7}{3} + \frac{\gamma}{Pr}\right) 2\omega \right]$$

Substituting this expression into $\Re Q(\xi, \eta)$, we obtain a sixteenth-order polynomial with respect to η . This polynomial contains only even degrees, namely, 0, 2, 4, 6, 8, 10, 12, 14, and 16. It is possible to make sure (we always use *Mathematica* (ref. 21) to perform cumbersome transformations) that the coefficients of the above polynomial are positive for all ω ($\omega \neq 0$) and for all Re ; consequently, the corresponding sixteenth-order equation has no real roots. Therefore, the determinant (eq. (18)) has no other real zeros in this case as well.

We have finally come to the most complicated case, which so far allows us only approximate investigation. Let $M_0^2 < \left(\frac{4}{3} + \frac{1}{Pr}\right)\left(\frac{7}{3} + \frac{\gamma}{Pr}\right)^{-1}$. Then, we have to clarify whether the functions $\Re Q(\xi_3^{(1)}(\eta), \eta)$ and/or $\Re Q(\xi_3^{(2)}(\eta), \eta)$ turn into zero for η within the range given in inequality (22). Both functions are actually of a general algebraic type (they contain non-integer powers), which means we have only a remote possibility of accurately (analytically) showing that they have no real roots, particularly because these functions depend on many parameters. At least at this point we are unable to construct the corresponding rigorous proof; therefore, we use the following graphical approach.

To start, we select some representative discrete set of the parameters involved. The range for the Mach number is known, so we simply choose a few points within this range. As for the Reynolds number, the representative values for the graphical tests we are conducting may be chosen to be about a few thousand. Indeed, we are not studying Stokes' flows that correspond to very low Re . As for typical laminar solutions for the flows around an airfoil, they apparently cease to exist starting with Reynolds numbers at around a few thousand. Moreover, for turbulent flows with true molecular Reynolds numbers of a few million, one can successfully model turbulence in the far field by introducing a new effective value of the Reynolds number, which also appears to be around a few thousand. (See ref. 12.) Finally, recall that the periodicity of flow in time is caused by some external influence, and reference 7 reports that the maximum effect (i.e., response) of such an influence corresponds to nondimensional frequencies of about 1. Therefore, we will not consider frequencies much less than unity or much greater than unity. The upper bound for the band of frequencies originates from the numerics since we are going to pass from series (6) to the finite Fourier series while actually solving the problem on the computer. (See section 3.)

We also note that the limits for η (see inequality (22)) do not depend on the sign of ω . Moreover, since $\xi_3^{(1)}(\eta, M_0, Re, Pr, \gamma, |\omega|) = -\xi_3^{(2)}(\eta, M_0, Re, Pr, \gamma, -|\omega|)$, $\xi_3^{(2)}(\eta, M_0, Re, Pr, \gamma, |\omega|) = -\xi_3^{(1)}(\eta, M_0, Re, Pr, \gamma, -|\omega|)$ (eq. (20)), and all powers of ξ and $(\omega + \xi)$ in $\Re Q(\xi, \eta)$ are even, it suffices to investigate the behavior of only one of the above functions for both positive and negative values of ω . We do this by plotting the corresponding graphs for the following specific values of the parameters involved: $\omega = \pm 0.5, \pm 1, \pm 10$, and ± 50 ; $M_0 = 0.4$ and 0.7 ; $Re = 1000, 2000$, and 5000 ; and γ and Pr are still 1.4 and 0.72 , respectively. The graphs drawn with the help of *Mathematica* (ref. 21) in different scales show that neither of the above curves intersects the real axis. (We do not present these plots here because they are not of interest except to show that the corresponding curve has no zeros). Relying on this approximate graphical investigation, we may expect that at least within some range of the parameters involved the symbol Q (eq. (16)) has no other real singular points, except for those that have already been found.

We use an analogous graphical approach for the case $M_0^2 > \left(\frac{4}{3} + \frac{1}{Pr}\right)\left(\frac{7}{3} + \frac{\gamma}{Pr}\right)^{-1}$. We have no prescribed range for η in this case. However, it is clear that the asymptotics of the functions $\Re Q(\xi_3^{(1,2)}(\eta), \eta)$ for large η is η^8 , so it suffices to study the behavior of the above functions only on some finite interval of η . We used *Mathematica* (ref. 21) to plot the corresponding graphs for the same values of ω, Re, γ , and Pr as mentioned before and for $M_0 = 0.8$ and 0.9 . The graphs (drawn in different scales for different η -intervals, up to $-10^5 < \eta < 10^5$) show that neither of the curves has real zeros in this case as well.

Summarizing, we conclude that at least for a certain reasonable range of the parameters involved, M_0, Re, Pr, γ , and ω , we have justified the following proposition.

Proposition 1: *The symbol $Q(\xi, \eta)$ (eq. (16)) has only three real singular points on the (ξ, η) -plane:*

$(-\omega, 0)$, $\left(\frac{\omega M_0}{1 - M_0}, 0\right)$, and $\left(-\frac{\omega M_0}{1 + M_0}, 0\right)$. For $\omega = 0$, these three points merge into one.

To determine whether the inverse symbol $Q^{-1}(\xi, \eta)$ belongs to $L_{loc}^1(R^2)$, it suffices to investigate the behavior (integrability) of this matrix function near the three singularities. This investigation actually means that we have to check integrability of each of the 16 elements of $Q^{-1}(\xi, \eta)$. These elements are given by $(Q^{-1})_{j,i} = \delta_{i,j}/Q$, $1 \leq i, j \leq 4$, where $\delta_{i,j}$ are the corresponding cofactors.

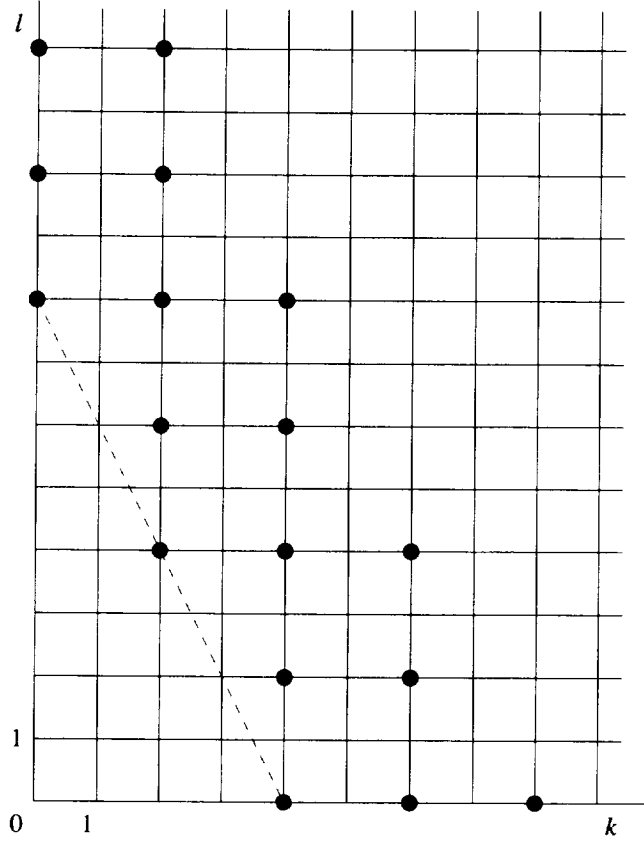


Figure 2. Powers involved in the denominator $Q\bar{Q}$ (black circles) and Newton's diagram (dashed line) for $Q\bar{Q}$; ($\xi = -\omega, \eta = 0$), $\omega \neq 0$.

Let us first concentrate on the singularity ($\xi = -\omega, \eta = 0$) for $\omega \neq 0$. We replace the above expressions for the elements of inverse symbol by their equivalents, $(Q^{-1})_{j,i} = (\delta_{i,j}\bar{Q})/(Q\bar{Q})$ (\bar{Q} means complex conjugate), to make the denominator purely real. Since both the denominator $Q\bar{Q}$ and the numerator $\delta_{i,j}\bar{Q}$ are the sums of monomials of the type $const \cdot (\omega + \xi)^k \eta^l \xi^m$ (here $const$ depends on M_0, Re, Pr, γ , and ω , and k, l, m are nonnegative integers), then it would be sufficient to make sure that any expression of the sort

$$\frac{|const \cdot (\omega + \xi)^k \eta^l \xi^m|}{Q\bar{Q}} \quad (24)$$

that originates from $(\delta_{i,j}\bar{Q})/(Q\bar{Q})$, $1 \leq i, j \leq 4$, is integrable near ($\xi = -\omega, \eta = 0$). Since $\omega \neq 0$, then the factors ξ^m do not contribute to the asymptotic behavior of expression (24) near ($\xi = -\omega, \eta = 0$), which is an essential difference in comparison with the case $\omega = 0$. (See the following discussion.) Therefore, we may investigate this asymptotic behavior by constructing Newton's diagram (see ref. 22 by Walker) with respect to only two variables, $\omega + \xi$ and η . Namely, we show in figure 2 the set of points (k, l) that correspond to all monomials $const \cdot (\omega + \xi)^k \eta^l \xi^m$ involved in $Q\bar{Q}$. The *Newton diagram* (ref. 22) is a lower part of the convex hull of the above set. The diagram is shown by the dashed line in figure 2. Those points (k, l) which belong to the Newton diagram determine the asymptotic behavior of $Q\bar{Q}$ near ($\xi = -\omega, \eta = 0$).

More precisely, the asymptotic behavior of $Q\bar{Q}$ near the singularity is determined not only by the lowest degree monomials (see Newton's diagram in fig. 2) but may also depend on some higher order terms if the form

$$A_Q^{(\omega)} \stackrel{\text{def}}{=} \frac{\xi^4}{M_0^4}(\omega + \xi)^4 + \frac{16}{9} \frac{\xi^4}{Re^4 Pr^2 M_0^4} \eta^8 + \frac{\xi^4}{Re^2 M_0^4} \left[\left(\frac{4}{3} + \frac{1}{Pr} \right)^2 - \frac{8}{3Pr} \right] (\omega + \xi)^2 \eta^4 \quad (25)$$

(which corresponds just to the previously mentioned lowest degree terms that constitute the Newton diagram) degenerates under some conditions. However, in this specific case the form $A_Q^{(\omega)}$ (eq. (25)) is positive definite because $\left[\left(\frac{4}{3} + \frac{1}{Pr} \right)^2 - \frac{8}{3Pr} \right]$ is positive for any Pr . Therefore, after some natural change of variables (see the following text) the asymptotic behavior of the denominator $Q\bar{Q}$ becomes uniform with respect to the polar angle, which implies that while investigating the integrability of $Q^{-1}(\xi, \eta)$ one may simply neglect all the higher-order terms (black circles above the dashed line on fig. 2) and consider the expression

$$\frac{|const \cdot (\omega + \xi)^k \eta^l \xi^m|}{A_Q^{(\omega)}} \quad (26)$$

instead of equation (24). Furthermore, we may only increase the ratio (eq. (26)) by neglecting the third term $(-\omega + \xi)^2 \eta^4$ in equation (25). Indeed, it is easy to see that in doing so we only decrease the denominator but still preserve its positive definiteness. Finally, eliminate the factors ξ^m , for simplicity. We have already mentioned that ξ^m do not contribute to asymptotics near $(\xi = -\omega, \eta = 0)$, $\omega \neq 0$. Therefore, to estimate the integrals, we may replace these factors by appropriate constants, e.g.,

$$\frac{|const \cdot (\omega + \xi)^k \eta^l \xi^m|}{(\xi^4/M_0^4)(\omega + \xi)^4 + (16/9)(\xi^4/Re^4 Pr^2 M_0^4)\eta^8} \leq \frac{|const \cdot (\omega + \xi)^k \eta^l| |\xi|_{\max}^m}{(\xi_{\min}^4/M_0^4)(\omega + \xi)^4 + (16/9)(\xi_{\min}^4/Re^4 Pr^2 M_0^4)\eta^8}$$

where minimum (min) and maximum (max) are found on a sufficiently small neighborhood of $(\xi = -\omega, \eta = 0)$.

Thus, we have reduced the original question of integrability of $(\delta_{i,j} Q)/(\bar{Q})$ to checking the integrability of the following function:

$$\frac{|const \cdot (\omega + \xi)^k \eta^l|}{a(\omega + \xi)^4 + b\eta^8} \quad (a > 0; b > 0; k, l \text{ are nonnegative integers}) \quad (27)$$

on some neighborhood of $(\xi = -\omega, \eta = 0)$. Because of the symmetry, it suffices to integrate function (27) only on one quadrant, for example, $\omega + \xi \geq 0$ and $\eta \geq 0$. Moreover, since we are studying local integrability, we also introduce some upper limits for $\omega + \xi$ and for η , e.g., $\omega + \xi \leq 1$ and $\eta \leq 1$. Let us now change the variables $\sqrt{a}(\omega + \xi)^2 = \zeta$ and $\sqrt{b}\eta^4 = \chi$ and then proceed to the following integral:

$$const \int_0^1 \int_0^1 \frac{\zeta^{(k-1)/2} \chi^{(l-3)/4}}{\zeta^2 + \chi^2} d\zeta d\chi \quad (28)$$

Further, make another change of variables, from Cartesian (ζ, χ) to polar (ρ, θ) coordinates, and for simplicity, truncate our rectangular domain, $\{0 \leq \zeta \leq 1, 0 \leq \chi \leq 1\} \rightarrow \{\zeta^2 + \chi^2 \leq 1\}$, which obviously does not influence the result (integrable or not integrable). Finally, we obtain, instead of integral (28),

$$const \int_0^1 \frac{\rho^{1+(k-1)/2+(l-3)/4}}{\rho^2} \int_0^{\pi/2} (\cos \theta)^{(k-1)/2} (\sin \theta)^{(l-3)/4} d\theta d\rho \quad (29)$$

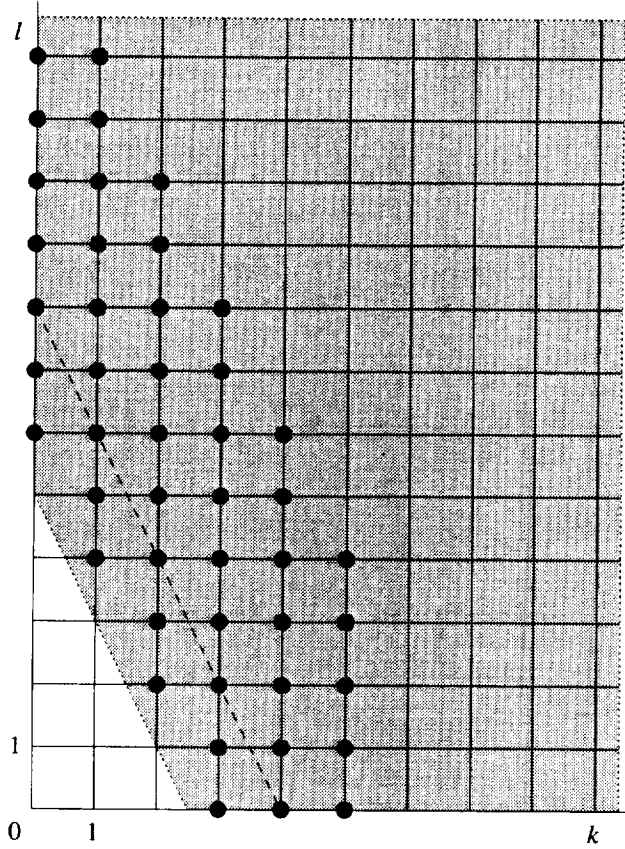


Figure 3. Black circles represent powers of the monomials in cofactors for $(\xi = -\omega, \eta = 0)$, $\omega \neq 0$. Gray area corresponds to integrability conditions (30).

From formula (29) one can easily derive the conditions sufficient for the integral to exist. Namely, they are

$$\frac{k-1}{2} + \frac{l-3}{4} > \varepsilon \quad (30a)$$

$$\frac{k-1}{2} > \varepsilon - 1 \quad (30b)$$

$$\frac{l-3}{4} > \varepsilon - 1 \quad (30c)$$

where ε is an arbitrarily small positive number.

We now have to make sure that all conditions (30) are satisfied for all cofactors $\delta_{i,j}$, $1 \leq i, j \leq 4$. First, we note that since k and l are always nonnegative integers, then two conditions (eqs. (30b) and (30c)) are met automatically. Then, to check the fulfillment of the third condition (eq. (30a)) one has to accurately calculate all monomials involved in all cofactors $\delta_{i,j}$, $1 \leq i, j \leq 4$ and analyze the powers (k, l) for $(\omega + \xi)^k \eta^l$. This step was done with the help of *Mathematica*. (See ref. 21.) In figure 3, we have collected all the relevant powers (k, l) for all cofactors $\delta_{i,j}$, $1 \leq i, j \leq 4$. We also show in figure 3 the range of powers (k, l) which satisfies conditions (30) (gray area). Using figure 3, one can easily conclude that all monomials involved satisfy all conditions (30). Therefore, the inverse symbol $\mathbf{Q}^{-1}(\xi, \eta)$ is absolutely integrable near the singular point $(\xi = -\omega, \eta = 0)$ for $\omega \neq 0$.

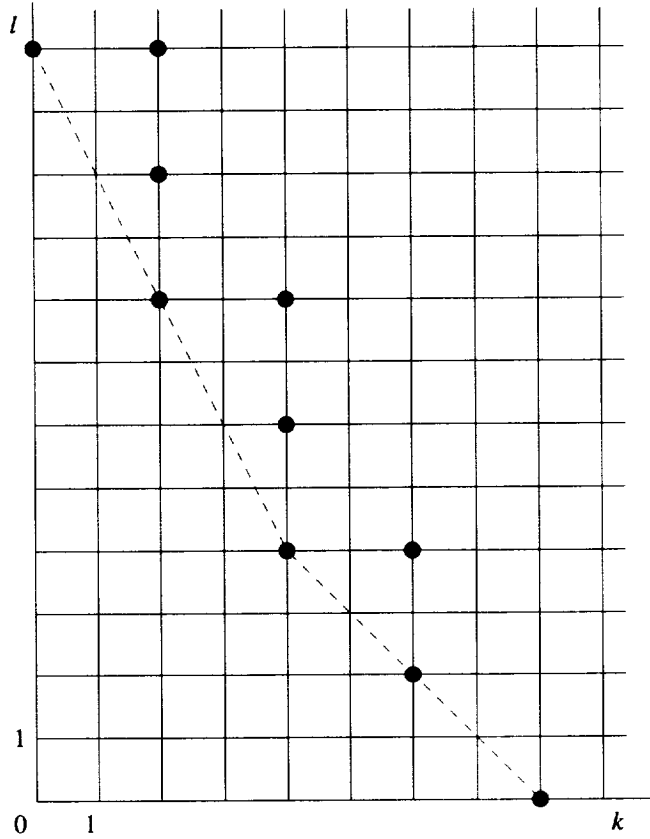


Figure 4. Powers involved in the denominator $Q\bar{Q}$ (black circles) and Newton's diagram (dashed line) for $Q\bar{Q}$; ($\xi = 0, \eta = 0$), $\omega \neq 0$.

The integrability of $Q^{-1}(\xi, \eta)$ for $\omega = 0$ near the singular point ($\xi = 0, \eta = 0$) is investigated by the same method. We only note that since ξ and $\omega + \xi$ are now the same, both of them do contribute to the asymptotic behavior of $Q^{-1}(\xi, \eta)$ near ($\xi = 0, \eta = 0$). Therefore, the sets of monomials involved, as well as the Newton diagram, for $Q\bar{Q}$ will differ noticeably from those relevant to the case $\omega \neq 0$. Indeed, the asymptotic behavior of the denominator $Q\bar{Q}$ near ($\xi = 0, \eta = 0$) is now determined by the following form (compare with expression (25)):

$$A_Q^{(0)} = \left(1 + \frac{1}{M_0^4} - \frac{2}{M_0^2}\right)\xi^8 + \frac{\eta^{12}}{M_0^4 Pr^2 Re^4} + \left(\frac{2}{M_0^4} - \frac{2}{M_0^2}\right)\xi^6 \eta^2 + \frac{1}{M_0^4} \xi^4 \eta^4 + \frac{1}{M_0^4 Re^2} \left[\left(1 + \frac{1}{Pr}\right)^2 - \frac{2}{Pr} \right] \xi^2 \eta^8 \quad (31)$$

which corresponds to the Newton diagram presented in figure 4.

As in the case $\omega \neq 0$, the form $A_Q^{(0)}$ (eq. (31)) also appears to be positive definite since all five coefficients in expression (31) are positive for all Re, Pr , and $M_0 < 1$. However, the Newton diagram shown in figure 4 consists of two straight intervals, whereas the one in figure 2 contains only one interval. This difference is essential because now each of the aforementioned two intervals (see the two-component dashed polygonal line in fig. 4) will determine its own domain of integrability for the expressions

$$\frac{|const \cdot \xi^k \eta^l|}{A_Q^{(0)}} \quad (32)$$

on the (k, l) -plane. Here k and l are the powers in the numerator of expression (32). Since the form $A_Q^{(0)}$ is not simply positive definite, but all powers involved are even, and each coefficient in formula (31) is positive, we can find the corresponding domain of integrability on the (k, l) -plane independently for each of the two parts of the Newton diagram. (See fig. 4.) To do this for either part of the diagram, neglect those terms in the denominator which correspond to another part (in so doing, the denominator may only decrease). Then, formally divide both the numerator and the denominator by the common factor ξ^4 . Using the changes of variables analogous to those previously implemented, we come to the following set of conditions sufficient for the integrability of function (32) near $(\xi = 0, \eta = 0)$:

$$\frac{k-1}{2} + \frac{l-7}{4} > \varepsilon \quad (33a)$$

$$\frac{k-1}{2} > \varepsilon - 1 \quad (33b)$$

$$\frac{l-7}{4} > \varepsilon - 1 \quad (33c)$$

and

$$\frac{k-5}{2} + \frac{l-1}{2} > \varepsilon \quad (34a)$$

$$\frac{k-5}{2} > \varepsilon - 1 \quad (34b)$$

$$\frac{l-1}{2} > \varepsilon - 1 \quad (34c)$$

Note that three conditions (eqs. (33)) correspond to the upper part of the Newton diagram and three conditions (eqs. (34)) correspond to its lower part. (See fig. 4.)

In figure 5, we show (with black circles) all powers (k, l) involved in all cofactors $\delta_{i,j}$, $1 \leq i, j \leq 4$ for the case $\omega = 0$. Gray areas on this figure correspond to the range of those coefficients (k, l) which satisfy integrability conditions (33) and (34). Note that conditions (33c) and (34b) impose some additional restrictions on l and k for the upper and lower components respectively of the Newton diagram in figure 5. We did not have such restrictions in the case $\omega \neq 0$. (See inequalities (30).) One can easily see from figure 5 that all elements of \mathbf{Q}^{-1} , $(\delta_{i,j}\bar{Q})/(Q\bar{Q})$, $1 \leq i, j \leq 4$, are absolutely integrable near $(\xi = 0, \eta = 0)$ in the case $\omega = 0$ as well.

Finally, we only have to show that $\mathbf{Q}^{-1}(\xi, \eta)$ is absolutely integrable on some neighborhood of each of the singular points $\left(\frac{\omega M_0}{1-M_0}, 0\right)$ and $\left(-\frac{\omega M_0}{1+M_0}, 0\right)$ for $\omega \neq 0$. If we simply ensure that $|Q^{-1}(\xi, \eta)|$ is

integrable on the same neighborhood, then the integrability of $\mathbf{Q}^{-1}(\xi, \eta)$ follows. To do this, first note that $\text{grad } Q(\xi, \eta) \neq \mathbf{0}$ at either of these two points. Indeed, it is quite easy to see from equation (18) that

$\frac{\partial Q}{\partial \xi} \neq 0$ at both $\left(\frac{\omega M_0}{1-M_0}, 0\right)$ and $\left(-\frac{\omega M_0}{1+M_0}, 0\right)$ for all $M_0 < 1$. Then, refer to reference 23, wherein

Vainberg proves exactly the same statement we need, namely, the integrability of $|Q^{-1}(\xi, \eta)|$ on some neighborhood of an isolated real zero of the polynomial $Q(\xi, \eta)$ when $\text{grad } Q(\xi, \eta) \neq \mathbf{0}$ at this point.

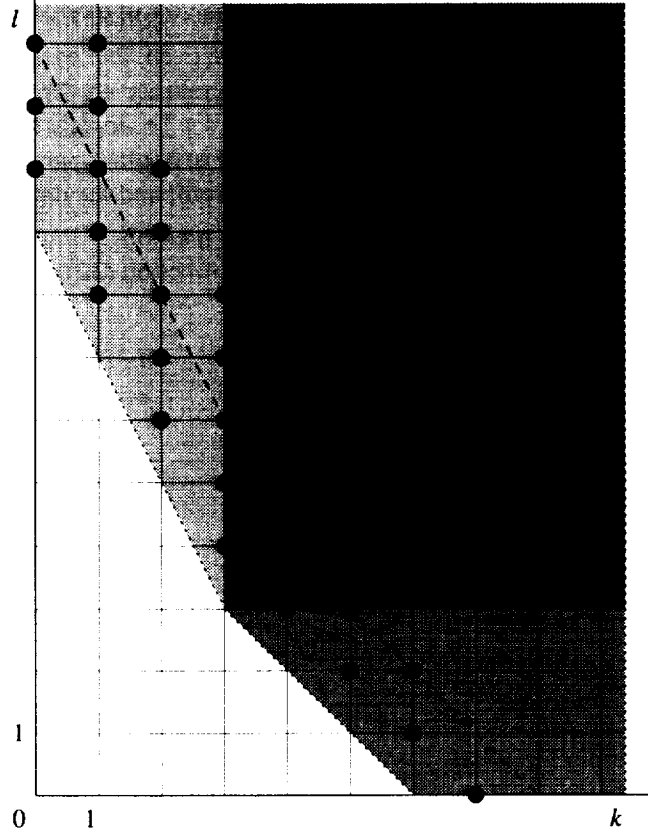


Figure 5. Black circles represent powers of the monomials in cofactors for $(\xi = 0, \eta = 0)$, $\omega \neq 0$. Light-gray area corresponds to integrability conditions (33). Middle-gray area corresponds to integrability conditions (34). Dark-gray area is common to both conditions (33) and (34).

Thus, we can finally formulate the following proposition.

Proposition 2: *The inverse symbol $\mathbf{Q}^{-1}(\xi, \eta)$ (eq. (16)) is absolutely integrable on any finite domain of \mathbb{R}^2 , i.e., $\mathbf{Q}^{-1}(\xi, \eta) \in L^1_{loc}(\mathbb{R}^2)$.*

In accordance with reference 20, proposition 2 immediately implies proposition 3.

Proposition 3 (existence): *The system (15) is solvable in \mathcal{G}' for any compactly supported $\hat{\mathbf{f}} \in L^1(\mathbb{R}^2)$; $\hat{\mathbf{f}}$ in equation (15) is a Fourier transform of $\hat{\mathbf{f}}$ (eq. (14b)).*

The solution to the AP (eqs. (12) and (13)) that we are looking for may generally be found by means of the inverse Fourier transform (again, the superscript n is omitted below),

$$\hat{\mathbf{u}}(x, y) = \frac{1}{2\pi} \int_{-\infty}^{\infty} \int_{-\infty}^{\infty} \hat{\mathbf{u}}(\xi, \eta) e^{i\xi x + i\eta y} d\xi d\eta \quad (35)$$

Using the brief notation, we may rewrite formula (35) as $\hat{\mathbf{u}} = (\hat{\mathbf{u}})^\vee = (\mathbf{Q}^{-1}\hat{\mathbf{f}})^\vee$. However, in doing so we still do not know whether the function $\hat{\mathbf{u}}(x, y)$ (eq. (35)) satisfies boundary condition (13). Let us first prove the following proposition.

Proposition 4 (uniqueness): *If the solution $\hat{\mathbf{u}}$ of system (12) satisfies the boundary condition (13), then it is unique in the class of distributions vanishing at infinity.*

Indeed, any function $\hat{\mathbf{u}}$ that solves system (12) is actually an inverse Fourier transform of some solution to system (15), $\hat{\mathbf{u}} = (\hat{\mathbf{u}})^\vee$. In turn, any distribution $\hat{\mathbf{u}} \in \mathcal{G}'$ that solves system (15) (see formula (17)) should coincide with the regular function $\mathbf{Q}^{-1}(\xi, \eta)\hat{\mathbf{f}}(\xi, \eta)$ everywhere on \mathcal{R}^2 except at the three singular points of $\mathbf{Q}(\xi, \eta)$ (since $\hat{\mathbf{f}}(\xi, \eta)$ has no singular points). Therefore, any other solution to system (15) may differ from $\hat{\mathbf{u}}$ only by a distribution with the support belonging to the three-point set $\left\{(-\omega, 0), \left(\frac{\omega M_0}{1 - M_0}, 0\right), \left(-\frac{\omega M_0}{1 + M_0}, 0\right)\right\}$. Such a distribution may be only a finite sum of δ -functions and

their derivatives. (See ref. 20.) Therefore, if $\hat{\mathbf{u}} = (\hat{\mathbf{u}})^\vee$ vanishes at infinity, then any other solution to system (12) will differ from $\hat{\mathbf{u}}$ by an inverse Fourier transform of a finite sum of δ -functions and their derivatives, and, consequently, it will not vanish at infinity since Fourier transforms of δ -functions and their derivatives are polynomials. (See ref. 20.) Thus, proposition 4 is justified.

Let us now select a finite ball B where

$$B \subset \mathcal{R}^2, B - \varepsilon \supset \left\{(-\omega, 0), \left(\frac{\omega M_0}{1 - M_0}, 0\right), \left(-\frac{\omega M_0}{1 + M_0}, 0\right)\right\} \quad (\varepsilon > 0)$$

and construct a partition of unity, $\mathbf{1} = \mathbf{g}_B + \mathbf{g}_{\bar{B}}$, where the functions \mathbf{g}_B and $\mathbf{g}_{\bar{B}}$ are infinitely smooth and bounded on \mathcal{R}^2 . The function \mathbf{g}_B is identically zero outside the ball $B + \varepsilon$, therefore, $\mathbf{g}_{\bar{B}}$ is identically zero inside the ball $B - \varepsilon$. Note that such functions always exist. (See, e.g., ref. 20.) Obviously, $\hat{\mathbf{u}} = (\mathbf{Q}^{-1}\hat{\mathbf{f}})^\vee = (\mathbf{Q}^{-1}\mathbf{g}_B\hat{\mathbf{f}})^\vee + (\mathbf{Q}^{-1}\mathbf{g}_{\bar{B}}\hat{\mathbf{f}})^\vee$. We will separately analyze each term on the right-hand side of the above sum. First, it is clear that $\mathbf{Q}^{-1}\mathbf{g}_B\hat{\mathbf{f}} \in L^1(\mathcal{R}^2)$ because $\hat{\mathbf{f}}$ is bounded and $\mathbf{Q}^{-1} \in L^1_{loc}(\mathcal{R}^2)$.

Therefore, $(\mathbf{Q}^{-1}\mathbf{g}_B\hat{\mathbf{f}})^\vee \rightarrow 0$ while $\sqrt{x^2 + y^2} \rightarrow \infty$. For the second term $(\mathbf{Q}^{-1}\mathbf{g}_{\bar{B}}\hat{\mathbf{f}})^\vee$ we cannot yet construct a general proof of its decay at infinity. The difficulties here arise from the fact that $\mathbf{Q}^{-1} \in L^1_{loc}(\mathcal{R}^2)$ but $\mathbf{Q}^{-1} \notin L^1(\mathcal{R}^2)$, i.e., it is not absolutely integrable near infinity. Therefore, a general proof may require an appropriate regularization of the corresponding oscillatory integral. However, we retain this question for a future investigation. For the time being, we can formulate the following two statements. Each will address the vanishing of the solution at infinity for some particular case (or in a weaker formulation).

First, assume that $\hat{\mathbf{f}} \in L^2(\mathcal{R}^2)$, which is actually not restrictive for our purposes. Then, $\hat{\mathbf{f}} \in L^2(\mathcal{R}^2)$ (we may treat the Fourier transform here in the sense of Plancherel, ref. 24). As mentioned before, $\mathbf{Q}^{-1} \notin L^1(\mathcal{R}^2)$; however, $\mathbf{Q}^{-1}\mathbf{g}_{\bar{B}}$ can be shown to be bounded on \mathcal{R}^2 . Therefore, $\mathbf{Q}^{-1}\mathbf{g}_{\bar{B}}\hat{\mathbf{f}} \in L^2(\mathcal{R}^2)$, which immediately yields $(\mathbf{Q}^{-1}\mathbf{g}_{\bar{B}}\hat{\mathbf{f}})^\vee \in L^2(\mathcal{R}^2)$. Thus, in this case the solution $\hat{\mathbf{u}}$ to system (12) is represented as a sum of two terms, $\hat{\mathbf{u}}^{(1)} + \hat{\mathbf{u}}^{(2)}$, where $\hat{\mathbf{u}}^{(1)} \rightarrow 0$ while $\sqrt{x^2 + y^2} \rightarrow \infty$ (true vanishing in the sense of boundary conditions (13) and $\hat{\mathbf{u}}^{(2)} \in L^2(\mathcal{R}^2)$, which may be treated as a “generalized decay”).

We also note here that the statement on uniqueness proven in proposition 4 also applies to the functions from $L^2(R^2)$ since the polynomials obviously do not belong to $L^2(R^2)$.

Second, if we impose some additional restrictions on $\hat{\mathbf{f}}$, namely, if we require that $\hat{\mathbf{f}}$ be sufficiently smooth on R^2 so that $\hat{\mathbf{f}} \in L^1(R^2)$, then we obtain a true decay for the second term as well, $(\mathbf{Q}^{-1} \mathbf{g}_B \hat{\mathbf{f}})^\vee \rightarrow 0$ while $\sqrt{x^2 + y^2} \rightarrow \infty$. Therefore, for a more particular class of the right-hand sides we may affirm that the problem (eqs. (12) and (13)) is uniquely solvable in \mathcal{G}' . We note that for some other cases (see ref. 9) such a restriction of the class of admissible right-hand sides does not influence the construction of a DPM-based numerical algorithm. We will not rigorously formulate and prove this statement for the specific case currently under study. However, we expect that this property does take place. These expectations are based on the numerical experience. (See refs. 8, 11, and 12.)

2.3. Truncation of Linearized Problem

As mentioned in section 2.1, we are not going to directly solve the problem (eqs. (8)–(10)). Instead, we will implement some additional truncation and further solve only a new finite substitute for the linearized problem. Since the problem (eqs. (8)–(10)) will be solved by means of the DPM, we must construct an equivalent finite substitute for the auxiliary problem (eqs. (12) and (13)). Moreover, the same finite substitute for the AP (eqs. (12) and (13)) will be used for calculating the operator \mathbf{P}_1^n , which provides boundary data for the problem (eqs. (8)–(10)). (See section 2.1.) In this section, we construct the finite substitute for the AP introducing some additional assumptions in regard to both the smoothness of the solution we are looking for as well as the rate of its decrease at infinity. This is done in order to simplify the presentation and to avoid unnecessary complications that are not essential for the purpose of constructing the numerical algorithm. We hope to provide a more rigorous analysis of the approach described here in a forthcoming paper.

For reasons of numerical convenience and effectiveness, we will use a different method for calculating the solution of the AP, rather than the one from section 2.2. Using this new solution technique, we will equivalently reformulate the AP on a new finite domain. Namely, let us again take the Fourier transform of both sides of system (12); however, now we do so only in one Cartesian direction, y (compare with eqs. (14)),

$$\hat{\mathbf{u}}(x, \eta) = \frac{1}{\sqrt{2\pi}} \int_{-\infty}^{\infty} \hat{\mathbf{u}}(x, y) e^{-i\eta y} dy \quad (36a)$$

$$\hat{\mathbf{f}}(x, \eta) = \frac{1}{\sqrt{2\pi}} \int_{-\infty}^{\infty} \hat{\mathbf{f}}(x, y) e^{-i\eta y} dy \quad (36b)$$

(Again, we drop the subscript n hereafter in this section to simplify the notation. Moreover, we retain here the same notation, $\hat{\mathbf{u}}$ and $\hat{\mathbf{f}}$, as in section 2.2; however, the left-hand sides of expressions (14) and (36) are obviously not the same.) Then, we obtain the following family of systems of ordinary differential equations (ODE's):

$$\frac{d\hat{\mathbf{u}}(x, \eta)}{dx} + \mathbf{Q}(\eta)\hat{\mathbf{u}}(x, \eta) = \tilde{\mathbf{f}}(x, \eta) \quad (37)$$

where

$$\mathbf{Q}(\eta) = \mathbf{D}^{-1} \begin{bmatrix} 0 & i\eta & 0 & i\omega \\ i\omega + \frac{\eta^2}{Re} & 0 & 0 & 0 \\ 0 & i\omega + \frac{4}{3} \frac{\eta^2}{Re} & i\eta & 0 \\ 0 & 0 & i\omega + \frac{\gamma\eta^2}{RePr} & -\frac{i\omega}{M_0^2} - \frac{\eta^2}{RePrM_0^2} \end{bmatrix}$$

and

$$\tilde{\mathbf{f}}(x, \eta) = \mathbf{D}^{-1} \hat{\mathbf{f}}(x, \eta)$$

(the matrix \mathbf{D} is defined in formula (36)). The family (eq. (37)) is parameterized by the continuous variable η , $-\infty < \eta < \infty$, and x is an independent variable. Recall that the solution $\hat{\mathbf{u}}(x, y)$ we are going to calculate should vanish at infinity. (See boundary conditions (13).) Consequently, we will generally impose the following boundary condition on the solution of system (37):

$$\hat{\mathbf{u}}_x, \eta \rightarrow 0 \text{ as } |x| \rightarrow \infty \quad (38a)$$

However, in particular cases (see the following discussion and ref. 8 for details) the condition (eq. (38a)) may appear too restrictive—namely, the cases when $\mathbf{Q}(\eta)$ has purely imaginary (or zero) eigenvalues. Therefore, for some selected values of ω and η we will only require

$$|\hat{\mathbf{u}}_x, \eta| \leq \text{const as } |x| \rightarrow \infty \quad (38b)$$

Note that we do not consider solutions that grow polynomially, the latter solutions correspond to the case when $\mathbf{Q}(\eta)$ has multiple purely imaginary eigenvalues and does not have a basis composed of eigenvectors.

Once we are able to find (for every η) a solution to system (37) that would satisfy boundary condition (38) at infinity, then the solution to the AP (eqs. (12) and (13)) can be restored by means of a one-dimensional inverse Fourier transform,

$$\hat{\mathbf{u}}(x, y) = \frac{1}{\sqrt{2\pi}} \int_{-\infty}^{\infty} \hat{\mathbf{u}}(x, \eta) e^{i\eta y} d\eta \quad (39)$$

Let us designate the inverse operator for the one-dimensional problem (eqs. (37) and (38)) by $\mathbf{G}_x(\eta)$. That is, the solution $\hat{\mathbf{u}}(x, \eta)$ to this problem is given by

$$\hat{\mathbf{u}}(x, \eta) = \mathbf{G}_x(\eta) \hat{\mathbf{f}}(x, \eta) \quad (40)$$

The operator $\mathbf{G}_x(\eta)$ is obviously linear. Combining formulas (36), (39), and (40), we obtain the following formula for the solution of the AP (eqs. (12) and (13)):

$$\hat{\mathbf{u}}(x, y) = \frac{1}{2\pi} \int_{-\infty}^{\infty} \mathbf{G}_x(\eta) \int_{-\infty}^{\infty} \hat{\mathbf{f}}(x, s) e^{-i(s-y)\eta} ds d\eta \quad (41a)$$

Now, we will show how one can pass from the AP (eqs. (12) and (13)) to the new AP formulated on the strip $\{-\infty < x < \infty\} \times \left\{-\frac{Y}{2} \leq y \leq \frac{Y}{2}\right\}$ and periodic in the y direction, with Y being the value of the period. In doing so, we expect that when the period Y grows, $Y \rightarrow \infty$, the solution to the new periodic AP will uniformly converge to the solution of the original AP (eqs. (12) and (13)) on any strip $\{-\infty < x < \infty\} \times \{-\dot{y} \leq y \leq \dot{y}\}$ where \dot{y} is fixed and always less than $Y/2$. We note that the same approach was used in reference 8 for the steady-state problems.

Hereafter, we assume that all functions involved are defined on the infinite strip $\{-\infty < x < \infty\} \times \left\{-\frac{Y}{2} \leq y \leq \frac{Y}{2}\right\}$. The width of the strip Y is initially supposed to be greater than the diameter of $\text{supp}\hat{\mathbf{f}}$. (Later we will consider the limit $Y \rightarrow \infty$.) We assume periodicity of the solution to the new AP in the y direction. Then the solution that vanishes as $|x| \rightarrow \infty$ is given by

$$\hat{\mathbf{u}}_Y(x, y) = \sum_{k=-\infty}^{k=\infty} \mathbf{G}_x\left(\frac{2\pi k}{Y}\right) \frac{1}{Y} \int_{-Y/2}^{Y/2} \hat{\mathbf{f}}(x, s) e^{-i\frac{2\pi k}{Y}(s-y)} ds \quad (41b)$$

In formula (41b), we use the Fourier series of a periodic function instead of the Fourier integral used in formula (41a). Our aim is to estimate $|\hat{\mathbf{u}}(x, y) - \hat{\mathbf{u}}_Y(x, y)|$ from above on a finite (fixed) interval $(-\dot{y}, \dot{y})$, $\dot{y} < Y/2$, uniformly with respect to x . Let us introduce a uniform mesh in η , where $h_\eta = 2\pi/Y$ is the mesh size, and designate $\eta_k = kh_\eta$, $k = 0, \pm 1, \pm 2, \dots$. Let us then fix some interval $(-\mathcal{A}, \mathcal{A})$; we will always choose h_η (and consequently Y) so that $\mathcal{A} = h_\eta(K + 1/2)$, K being an integer. Then,

$$\begin{aligned} |\hat{\mathbf{u}}(x, y) - \hat{\mathbf{u}}_Y(x, y)| &= \frac{1}{2\pi} \left| \int_{-\infty}^{\infty} \mathbf{G}_x(\eta) \int_{-\infty}^{\infty} \hat{\mathbf{f}}(x, s) e^{-i(s-y)\eta} ds d\eta - \sum_{k=-\infty}^{k=\infty} h_\eta \mathbf{G}_x(\eta_k) \int_{-Y/2}^{Y/2} \hat{\mathbf{f}}(x, s) e^{-i\eta_k(s-y)} ds \right| \\ &\leq \frac{1}{2\pi} \left| \int_{-\mathcal{A}}^{\mathcal{A}} \dots - \sum_{k=-K}^{k=K} \dots \right| + \frac{1}{2\pi} \left| \int_{|\eta| > \mathcal{A}} \dots - \sum_{|k| > K} \dots \right| = \frac{1}{2\pi} |\cdot|_1 + \frac{1}{2\pi} |\cdot|_2 \end{aligned}$$

Let us separately estimate each of the two terms (the first one corresponds to the finite interval, and the second one corresponds to the complementary infinite interval).

$$\begin{aligned} \frac{1}{2\pi} |\cdot|_1 &\leq \frac{1}{2\pi} \sum_{k=-K}^{k=K} \left| \int_{(K-1/2)h_\eta}^{(K+1/2)h_\eta} \mathbf{G}_x(\eta) \int_{-\infty}^{\infty} \hat{\mathbf{f}}(x, s) e^{-i(s-y)\eta} ds d\eta - h_\eta \mathbf{G}_x(\eta_k) \int_{-Y/2}^{Y/2} \hat{\mathbf{f}}(x, s) e^{-i\eta_k(s-y)} ds \right| \\ &\leq \frac{1}{2\pi} \sum_{k=-K}^{k=K} \left[\left| \int_{(K-1/2)h_\eta}^{(K+1/2)h_\eta} \mathbf{G}_x(\eta) \int_{-\infty}^{\infty} \hat{\mathbf{f}}(x, s) e^{-i(s-y)\eta} ds d\eta - h_\eta \mathbf{G}_x(\eta_k) \int_{-\infty}^{\infty} \hat{\mathbf{f}}(x, s) e^{-i\eta_k(s-y)} ds \right| \right. \\ &\quad \left. + h_\eta \left| \mathbf{G}_x(\eta_k) \int_{|s| > Y/2} \hat{\mathbf{f}}(x, s) e^{-i\eta_k(s-y)} ds \right| \right] \end{aligned}$$

Clearly, the right-hand side of this inequality is actually the sum of errors of the quadrature formula of rectangles for the function $\hat{\mathbf{u}}(x, \eta)e^{i\eta y} = \mathbf{G}_x(\eta) \int_{-\infty}^{\infty} \hat{\mathbf{f}}(x, s)e^{-i\eta(s-y)}ds$ (see formula (40)) on elementary segments of the kind $[(k - 1/2)h_\eta, (k + 1/2)h_\eta]$, $k = -K, \dots, K$. Indeed, for each k , $k = -K, \dots, K$, the third term that corresponds to the integration over $|s| > Y/2$ turns into zero for sufficiently large Y 's since $\hat{\mathbf{f}}(x, s)$ is compactly supported. Therefore, one can obtain the following estimate:

$$\begin{aligned} \frac{1}{2\pi}|\cdot|_1 &\leq \text{const} \cdot h_\eta^2 \mathcal{A} \max_{\substack{x \in R \\ \eta \in (-\mathcal{A}, \mathcal{A})}} \left| \frac{\partial^2}{\partial \eta^2} \left[\hat{\mathbf{u}}(x, \eta)e^{i\eta y} \right] \right| \\ &\leq \text{const} \cdot h_\eta^2 \mathcal{A} \max_{\substack{x \in R \\ \eta \in (-\mathcal{A}, \mathcal{A})}} \left[\left| \frac{\partial^2 \hat{\mathbf{u}}(x, \eta)}{\partial \eta^2} \right| + 2|y| \left| \frac{\partial \hat{\mathbf{u}}(x, \eta)}{\partial \eta} \right| + y^2 |\hat{\mathbf{u}}(x, \eta)| \right] \\ &= (c_1 + c_2|y| + c_3y^2)h_\eta^2 \mathcal{A} \quad (c_1, c_2, c_3 > 0) \end{aligned}$$

Note that if we initially assume that the solution $\hat{\mathbf{u}}(x, y)$ decreases at infinity sufficiently fast, then the differentiability of its Fourier transform $\hat{\mathbf{u}}(x, n)$ (see the right-hand side of the previous inequality) follows directly.

For the second expression, we obtain

$$\frac{1}{2\pi}|\cdot|_2 \leq \frac{1}{2\pi} \left[\int_{|\eta| > \mathcal{A}} \left| \mathbf{G}_x(\eta) \int_{-\infty}^{\infty} \hat{\mathbf{f}}(x, s)e^{-i\eta(s-y)}ds \right| d\eta + \sum_{|k| > K} h_\eta \left| \mathbf{G}_x(\eta_k) \int_{-Y/2}^{Y/2} \hat{\mathbf{f}}(x, s)e^{-i\eta(s-y)}ds \right| \right]$$

Let us replace the integration limits $\int_{-Y/2}^{Y/2}$ in the second term on the right-hand side of this inequality by $\int_{-\infty}^{\infty}$, as was done when estimating $|\cdot|_1$. Then,

$$\frac{1}{2\pi}|\cdot|_2 \leq \frac{1}{2\pi} \left[\int_{|\eta| > \mathcal{A}} |\hat{\mathbf{u}}(x, \eta)| d\eta + \sum_{|k| > K} h_\eta |\hat{\mathbf{u}}(x, \eta_k)| \right]$$

Additionally we assume that the solution we are looking for has two absolutely integrable derivatives. Then its Fourier transform decreases faster than $|\eta|^{-2}$ and the previous inequality straightly implies

$$\frac{1}{2\pi}|\cdot|_2 \leq \frac{c_4}{\mathcal{A}} \quad (c_4 > 0)$$

Combining the two obtained estimates, one easily gets

$$|\hat{\mathbf{u}}(x, y) - \hat{\mathbf{u}}_Y(x, y)| \leq c_0 h_\eta^2 \mathcal{A} + \frac{c_4}{\mathcal{A}}$$

where $c_0 \stackrel{\text{def}}{=} \max_{y \in (-\hat{y}, \hat{y})} (c_1 + c_2|y| + c_3y^2)$, $c_0 > 0$. Clearly, all constants involved in the foregoing estimates depend, generally speaking, on the specific nonperiodic function $\hat{\mathbf{u}}(x, y)$ that we approximate by the periodic functions $\hat{\mathbf{u}}_Y(x, y)$.

Now let ε be an arbitrary positive number. We will choose sufficiently large Y_ε (i.e., sufficiently small h_{η_ε}) so that the following inequality

$$c_0 h_\eta^2 \mathcal{A} + \frac{c_4}{\mathcal{A}} < \varepsilon \quad (42)$$

is satisfied for all $Y > Y_\varepsilon$. In other words, we require that for a prescribed ε and for any $h_\eta < h_{\eta_\varepsilon}$ inequality (42) has real positive solutions \mathcal{A} of the special kind, $\mathcal{A} = (K + 1/2)h_\eta$ (K being an integer). The latter requirement is always met if, e.g., the distance between the real roots of the quadratic equation $c_0 h_\eta^2 \mathcal{A}^2 - \varepsilon \mathcal{A} + c_4 = 0$ is greater than h_η . This, in turn, yields the inequality $\varepsilon^2 - 4c_0 c_4 h_\eta^2 - c_0^2 h_\eta^6 > 0$ for h_η . This inequality is obviously satisfied for any $0 \leq h_\eta < h_{\eta_\varepsilon}$, where $h_{\eta_\varepsilon} \in R$ is a unique positive root of the equation $\varepsilon^2 - 4c_0 c_4 h_\eta^2 - c_0^2 h_\eta^6 = 0$. Since the fulfillment of inequality (42) is sufficient for the estimate

$$|\hat{\mathbf{u}}(x, y) - \hat{\mathbf{u}}_Y(x, y)| < \varepsilon \quad (43)$$

to be true, then we have shown that for all $\varepsilon > 0$ one can always find a sufficiently large period Y_ε so that for any $Y > Y_\varepsilon$ the absolute value of the discrepancy between the nonperiodic solution $\hat{\mathbf{u}}(x, y)$ and its periodic approximation $\hat{\mathbf{u}}_Y(x, y)$, $|\hat{\mathbf{u}}(x, y) - \hat{\mathbf{u}}_Y(x, y)|$, does not exceed ε for all x and for all $-\dot{y} \leq y \leq \dot{y}$.

Thus, we have reduced the original AP (eqs. (12) and (13)) to the new AP formulated on the strip $\{-\infty < x < \infty\} \times \left\{-\frac{Y}{2} \leq y \leq \frac{Y}{2}\right\}$. In section 3, we show that we will only need to know the solution of the AP in some neighborhood of $\text{supp}\hat{\mathbf{f}}$, therefore, the approximation of the nonperiodic function $\hat{\mathbf{u}}(x, y)$ by a periodic one, $\hat{\mathbf{u}}_Y(x, y)$, *only on a finite interval* $-\dot{y} \leq y \leq \dot{y}$ is sufficient for our purposes. Let us now show how to pass from the domain $\{-\infty < x < \infty\} \times \left\{-\frac{Y}{2} \leq y \leq \frac{Y}{2}\right\}$, which is still infinite, to a truly finite domain for the new AP.

Instead of $\{-\infty < x < \infty\} \times \left\{-\frac{Y}{2} \leq y \leq \frac{Y}{2}\right\}$, let us now consider a rectangular domain $D_Y^0 = (0, X) \times (-Y/2, Y/2)$. (See fig. 1.) This new domain D_Y^0 should completely contain Γ and Γ_1 . We will reformulate the new AP so that its solution will be determined only on this finite domain D_Y^0 and will coincide there with the corresponding fragment of the solution found on $\{-\infty < x < \infty\} \times \left\{-\frac{Y}{2} \leq y \leq \frac{Y}{2}\right\}$ before the reformulation. As previously mentioned, we only need to calculate the solution to the AP in some neighborhood of D_{in} . Therefore, we are always able to choose an appropriate X and Y so that this neighborhood belongs to D_Y^0 , and consequently we only need to construct special boundary conditions at the lines $x = 0$ and $x = X$ so that the reformulated new AP being solved on D_Y^0 is equivalent to the periodic AP on the strip $\{-\infty < x < \infty\} \times \left\{-\frac{Y}{2} \leq y \leq \frac{Y}{2}\right\}$ described earlier in this section. These boundary conditions at $x = 0$ and $x = X$ will be set separately for each

wavenumber $k, k = 0, \pm 1, \pm 2, \dots$, (see formula (41b)) involved in the Fourier representation of the function $\hat{\mathbf{u}}_Y(x, y)$. Namely, for each $k, k = 0, \pm 1, \pm 2, \dots$, we require that the corresponding Fourier mode, $\hat{\mathbf{u}}(x, \eta_k) \equiv \hat{\mathbf{u}}(x, 2\pi k/Y)$, meets boundary condition (38) at infinity. To exactly transfer condition (38) from infinity to the finite boundaries $x = 0$ and $x = X$, we use the following consideration. Since system (37) consists of ODE's with constant coefficients and since it is homogeneous outside $(0, X)$ (recall that $\text{supp}\hat{\mathbf{f}}(x, y) \subset D_{in}$, and consequently $\text{supp}\hat{\mathbf{f}}(x, \eta) \subset (0, X)$ for all η), then it obviously has four linearly independent eigensolutions (in the region of homogeneity). Depending on the structure of the set of eigenvalues of the matrix $\mathbf{Q}(\eta)$, these eigensolutions may either increase or decrease (eq. (38a)) exponentially, or they may oscillate (eq. (38b)) while $x \rightarrow \infty$ and while $x \rightarrow -\infty$. As previously mentioned, we do not consider the last possible case when $\mathbf{Q}(\eta)$ has multiple purely imaginary (or zero) eigenvalues and does not have a basis composed of eigenvectors, which leads to polynomially growing solutions. Sometimes one can analytically make sure that this case really does not take place. For example, we do this in section 3 in the discrete formulation for some particular values of ω and η . In other situations, this question may require some additional numerical investigation as in reference 8. At any rate, to satisfy boundary condition (38), we must prohibit at $x = 0$ all solutions that do not decrease to the left (i.e., as $x \rightarrow -\infty$), and prohibit at $x = X$ all solutions that increase to the right (i.e., as $x \rightarrow \infty$). The reason for this asymmetry was mentioned before: once we have purely imaginary (or zero) eigenvalues of $\mathbf{Q}(\eta)$ and, consequently, oscillating or constant-in-space solutions (see formula (38b)), then we cannot always prohibit at both ends of the interval $(0, X)$ all modes that do not decrease in the corresponding direction. However, it should not affect the result since the final solution we are looking for ($\hat{\mathbf{u}}(x, y)$) decreases at infinity. (See subsection 2.2.) Moreover, we have proven in reference 8 that once we have a selected nondecreasing mode in Fourier representation of the solution, then after the inverse Fourier transform the entire solution will nevertheless decrease. Therefore, we can take into account selected nondecreasing modes (if any) by simply admitting them at one of the two boundaries, $x = 0$ or $x = X$. (In case we do not do this, the problem may appear overdetermined.) It seems more natural to admit the nondecreasing Fourier modes (if any) at the downstream boundary $x = X$. (See ref. 8.)

Now, we calculate the eigenvalues $\lambda_r(\eta_k), r = 1, \dots, 4$, for the matrix $\mathbf{Q}(\eta_k)$. Those eigensolutions that increase to the right correspond to eigenvalues $\Re\lambda_r < 0$, and those eigensolutions that do not decrease to the left correspond to eigenvalues $\Re\lambda_r \geq 0$. Therefore, the following boundary conditions at $x = 0$ and $x = X$ may be considered to provide an exact transfer of boundary condition (38) from infinity:

$$\mathbf{S}^-(\eta_k)\hat{\mathbf{u}}(0, \eta_k) = \mathbf{0} \quad (k = 0, \pm 1, \pm 2, \dots) \quad (44a)$$

$$\mathbf{S}^+(\eta_k)\hat{\mathbf{u}}(X, \eta_k) = \mathbf{0} \quad (k = 0, \pm 1, \pm 2, \dots) \quad (44b)$$

Here $\mathbf{S}^-(\eta_k)$ and $\mathbf{S}^+(\eta_k)$ are the special rank-deficient 4×4 matrices that depend on $\mathbf{Q}(\eta_k)$, with their ranks equal to the numbers of eigenvalues $\lambda_r(\eta_k)$ with nonnegative and negative real parts, respectively. These matrices are given by

$$\mathbf{S}^-(\eta_k) = \prod_{\Re\lambda_r(\eta_k) < 0} (\mathbf{Q}(\eta_k) - \lambda_r(\eta_k)\mathbf{I}) \quad (45a)$$

$$\mathbf{S}^+(\eta_k) = \prod_{\Re\lambda_r(\eta_k) \geq 0} (\mathbf{Q}(\eta_k) - \lambda_r(\eta_k)\mathbf{I}) \quad (45b)$$

Here \mathbf{I} is an identity matrix and products in formulas (45) are calculated in accordance with the multiplicities of the eigenvalues. Analogous conditions will be used in section 3 while dealing with the finite-difference formulation of the AP.

Thus, the formulation of the new finite AP is now complete. Namely, we have to solve equations (12) for the compactly supported right-hand side $\hat{\mathbf{f}}$ ($\text{supp} \hat{\mathbf{f}} \subset D_{in}$) on the domain D_Y^0 (see fig. 1) with the periodicity boundary conditions in the y direction (Y being the value of the period) and with boundary conditions (44a) and (45a) at $x = 0$ and (44b) and (45b) at $x = X$. In the next section, we proceed to the finite-difference formulation of the problem and describe the numerical algorithm for setting the global DPM-based ABC's.

3. Numerical Method

3.1. Finite-Difference Scheme

Let us introduce a uniform Cartesian grid in $D_Y^0 \times [0, T]$, with h_x , h_y , and τ being the sizes of the grid in x , y , and t directions, respectively. We designate this grid \mathcal{N}^{0T} ,

$$\begin{aligned} \mathcal{N}^{0T} = \{ (x_m, y_j, t_l) \equiv (mh_x, jh_y - Y/2, l\tau) \mid h_x, h_y, \tau > 0; \\ m = 0, 1, \dots, M, M = X/h_x; \quad j = 0, 1, \dots, 2J + 1, 2J + 1 = Y/h_y; \\ l = 0, 1, \dots, 2L + 1, 2L + 1 = T/\tau \} \end{aligned} \quad (46)$$

We will construct a second-order finite-difference approximation of the system (eq. (3a)) on the grid \mathcal{N}^{0T} (see formula (46)) using the stencil shown in figure 6.

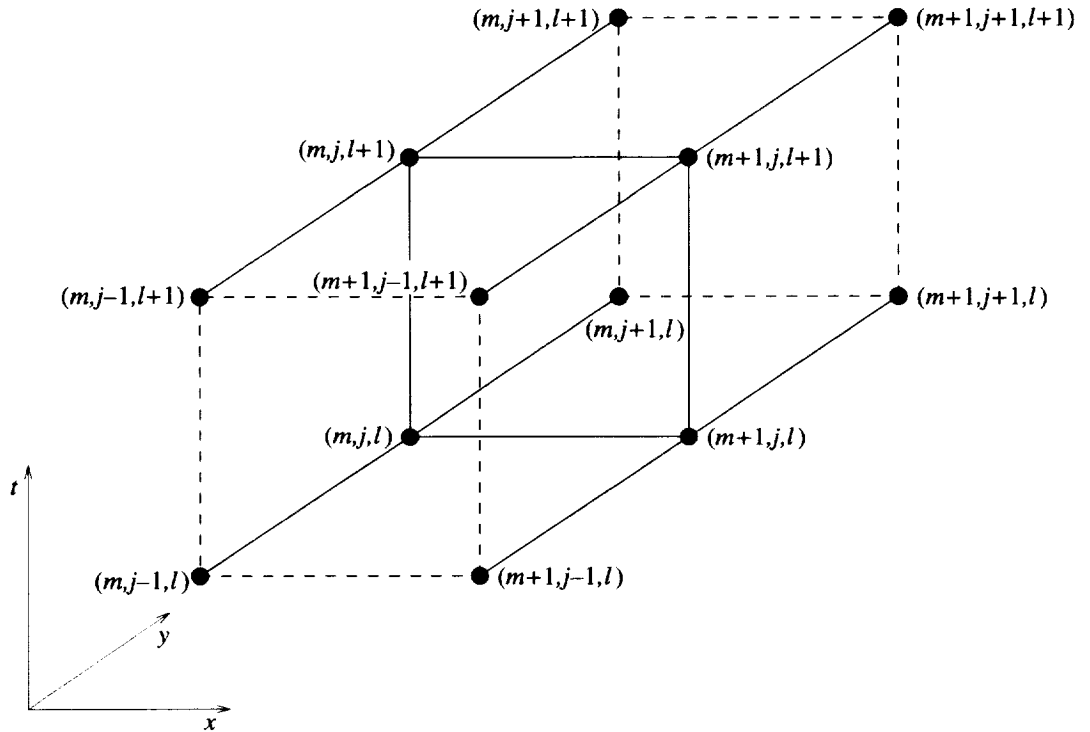


Figure 6. Stencil.

Namely, we use the first-order differences in the x and t directions and second-order central differences in the y direction, and we center the scheme with respect to the point $(m + 1/2, j, l + 1/2)$, which yields

$$\begin{aligned}
& \frac{1}{2} \mathbf{C} \left(\frac{\mathbf{u}_{m,j}^{l+1} - \mathbf{u}_{m,j}^l}{\tau} + \frac{\mathbf{u}_{m+1,j}^{l+1} - \mathbf{u}_{m+1,j}^l}{\tau} \right) + \frac{1}{2} \mathbf{D} \left(\frac{\mathbf{u}_{m+1,j}^{l+1} - \mathbf{u}_{m,j}^{l+1}}{h_x} + \frac{\mathbf{u}_{m+1,j}^l - \mathbf{u}_{m,j}^l}{h_x} \right) \\
& + \frac{1}{4} \mathbf{F} \left(\frac{\mathbf{u}_{m,j+1}^l - \mathbf{u}_{m,j-1}^l}{2h_y} + \frac{\mathbf{u}_{m+1,j+1}^l - \mathbf{u}_{m+1,j-1}^l}{2h_y} + \frac{\mathbf{u}_{m,j+1}^{l+1} - \mathbf{u}_{m,j-1}^{l+1}}{2h_y} + \frac{\mathbf{u}_{m+1,j+1}^{l+1} - \mathbf{u}_{m+1,j-1}^{l+1}}{2h_y} \right) \\
& + \frac{1}{4} \mathbf{H} \left(\frac{\mathbf{u}_{m,j+1}^l - 2\mathbf{u}_{m,j}^l + \mathbf{u}_{m,j-1}^l}{h_y^2} + \frac{\mathbf{u}_{m+1,j+1}^l - 2\mathbf{u}_{m+1,j}^l + \mathbf{u}_{m+1,j-1}^l}{h_y^2} \right. \\
& \left. + \frac{\mathbf{u}_{m,j+1}^{l+1} - 2\mathbf{u}_{m,j}^{l+1} + \mathbf{u}_{m,j-1}^{l+1}}{h_y^2} + \frac{\mathbf{u}_{m+1,j+1}^{l+1} - 2\mathbf{u}_{m+1,j}^{l+1} + \mathbf{u}_{m+1,j-1}^{l+1}}{h_y^2} \right) = \mathbf{0} \tag{47}
\end{aligned}$$

The finite-difference scheme (47) is written for the nodes (m, j, l) , $m = 0, 1, \dots, M-1$, $j = 0, 1, \dots, 2J$, $l = 0, 1, \dots, 2L$ with the assumption that we later impose periodicity boundary conditions in time as well as in the y direction. Note that the stability of the scheme of type (47) was examined for the model scalar equation

$$\frac{\partial u}{\partial t} + \frac{\partial u}{\partial x} + \frac{\partial u}{\partial y} = \frac{1}{Re^2} \frac{\partial^2 u}{\partial y^2} \tag{48}$$

It turns out that the corresponding finite-difference scheme for equation (48) is unconditionally stable in the von Neumann sense.

Then, using the periodicity conditions (compare with formula (4))

$$\mathbf{u}_{m,j}^0 = \mathbf{u}_{m,j}^{2L+1} \quad (m = 0, 1, \dots, M; j = 0, 1, \dots, 2J+1) \tag{49}$$

we implement a discrete Fourier transform in time (compare with formulas (7) and (6)),

$$\hat{\mathbf{u}}_{m,j}^n = \frac{1}{2L+1} \sum_{l=0}^{2L} \mathbf{u}_{m,j}^l e^{-inl\tau \frac{2\pi}{T}} \quad (m = 0, 1, \dots, M; j = 0, 1, \dots, 2J+1; n = -L, \dots, L) \tag{50}$$

$$\mathbf{u}_{m,j}^l = \sum_{n=-L}^L \hat{\mathbf{u}}_{m,j}^n e^{inl\tau \frac{2\pi}{T}} \quad (m = 0, 1, \dots, M; j = 0, 1, \dots, 2J+1; l = 0, 1, \dots, 2L) \tag{51}$$

and instead of system (47) obtain

$$\begin{aligned}
& \frac{s_n}{2} \mathbf{C} (\hat{\mathbf{u}}_{m,j}^n + \hat{\mathbf{u}}_{m+1,j}^n) + c_n \mathbf{D} \frac{\hat{\mathbf{u}}_{m+1,j}^n - \hat{\mathbf{u}}_{m,j}^n}{h_x} + \frac{c_n}{2} \mathbf{F} \left(\frac{\hat{\mathbf{u}}_{m,j+1}^n - \hat{\mathbf{u}}_{m,j-1}^n}{2h_y} + \frac{\hat{\mathbf{u}}_{m+1,j+1}^n - \hat{\mathbf{u}}_{m+1,j-1}^n}{2h_y} \right) \\
& + \frac{c_n}{2} \mathbf{H} \left(\frac{\hat{\mathbf{u}}_{m,j+1}^n - 2\hat{\mathbf{u}}_{m,j}^n + \hat{\mathbf{u}}_{m,j-1}^n}{h_y^2} + \frac{\hat{\mathbf{u}}_{m+1,j+1}^n - 2\hat{\mathbf{u}}_{m+1,j}^n + \hat{\mathbf{u}}_{m+1,j-1}^n}{h_y^2} \right) = 0 \tag{52}
\end{aligned}$$

Here $s_n = 2i \sin\left(\frac{1}{2}n\tau \frac{2\pi}{T}\right) / \tau$; $c_n = \cos\left(\frac{1}{2}n\tau \frac{2\pi}{T}\right)$; $n = -L, \dots, L$; $m = 0, 1, \dots, M-1$; and $j = 0, 1, \dots, 2J$.

The finite-difference system (52) is a discrete analogue of the continuous system (8) on the two-dimensional grid \mathcal{X}^0 ,

$$\begin{aligned} \mathcal{X}^0 &= \{(x_m, y_j) \equiv (mh_x, jh_y - Y/2) | h_x, h_y > 0; \\ m &= 0, 1, \dots, M, M = X/h_x; j = 0, 1, \dots, 2J + 1, 2J + 1 = Y/h_y\} \end{aligned} \quad (53)$$

In formula (53) h_x and h_y are the same as in formula (46).

We also note that once $\tau \rightarrow 0$, then $s_n \rightarrow i2\pi n/T = i\omega_n$ (see section 2) and $c_n \rightarrow 1$.

3.2. Difference Auxiliary Problem

Let us construct another Cartesian grid in D_Y^0 ,

$$\begin{aligned} \mathcal{M}^0 &= \{(x_{m+1/2}, y_j) \equiv ((m+1/2)h_x, jh_y - Y/2) | h_x, h_y > 0; \\ m &= 0, 1, \dots, M-1, M = X/h_x; j = 0, 1, \dots, 2J + 1, 2J + 1 = Y/h_y\} \end{aligned} \quad (54)$$

The grid sizes h_x and h_y are the same as before. The difference AP is formulated for the inhomogeneous counterpart of system (52) with a certain compactly supported right-hand side. The unknowns for the difference AP are defined on the grid \mathcal{X}^0 (see formula (53)), and the right-hand side is defined on the grid \mathcal{M}^0 . (See formula (54).) In doing so, we obviously have the second order of approximation. We will define the specific right-hand side for the AP, $\hat{\mathbf{f}}_{m+1/2, j}^n$, $m = 0, 1, \dots, M-1$, $j = 0, 1, \dots, 2J$, in section 3.3. As for now, assuming that this right-hand side is already known ($\text{supp} \hat{\mathbf{f}}_{m+1/2, j}^n \subset D_{in}$), we provide an exact formulation of the difference AP and describe an effective algorithm for its numerical solution.

In accordance with the results of section 2.3, we impose the periodicity boundary conditions in the y direction,

$$\hat{\mathbf{u}}_{m, 0}^n = \hat{\mathbf{u}}_{m, 2J+1}^n \quad (m = 0, 1, \dots, M) \quad (55a)$$

$$\hat{\mathbf{u}}_{m, -1}^n = \hat{\mathbf{u}}_{m, 2J}^n \quad (m = 0, 1, \dots, M) \quad (55b)$$

Then, we implement a discrete Fourier transform (compare with formulas (36)),

$$\hat{\mathbf{u}}_{m, k}^n = \frac{1}{2J+1} \sum_{j=0}^{2J} \hat{\mathbf{u}}_{m, j}^n e^{-ikjh_y \frac{2\pi}{Y}} \quad (m = 0, 1, \dots, M; k = -J, \dots, J) \quad (56a)$$

$$\hat{\mathbf{f}}_{m+1/2, k}^n = \frac{1}{2J+1} \sum_{j=0}^{2J} \hat{\mathbf{f}}_{m+1/2, j}^n e^{-ikjh_y \frac{2\pi}{Y}} \quad (m = 0, 1, \dots, M-1; k = -J, \dots, J) \quad (56b)$$

and obtain, instead of the inhomogeneous counterpart to system (52),

$$\mathbf{A}_k^n \hat{\mathbf{u}}_{m+1, k}^n + \mathbf{B}_k^n \hat{\mathbf{u}}_{m, k}^n = \hat{\mathbf{f}}_{m+1/2, k}^n \quad (m = 0, 1, \dots, M-1; k = -J, \dots, J) \quad (57)$$

where the 4×4 matrices \mathbf{A}_k^n and \mathbf{B}_k^n are given by

$$\mathbf{A}_k^n = \frac{s_n}{2} \mathbf{C} + \frac{c_n}{h_x} \mathbf{D} + \frac{c_n r_k}{2} \mathbf{F} + \frac{c_n t_k}{2} \mathbf{H} \quad (58a)$$

$$\mathbf{B}_k^n = \frac{s_n}{2} \mathbf{C} - \frac{c_n}{h_x} \mathbf{D} + \frac{c_n r_k}{2} \mathbf{F} + \frac{c_n t_k}{2} \mathbf{H} \quad (58b)$$

Here $r_k = i \sin\left(kh_y \frac{2\pi}{Y}\right)/h_y$, $t_k = -4 \sin^2\left(\frac{1}{2}kh_y \frac{2\pi}{Y}\right)/h_y^2$, and \mathbf{C} , \mathbf{D} , \mathbf{F} , and \mathbf{H} are defined in formula (3b). For each wavenumber k , $k = -J, \dots, J$, system (57) is composed of ordinary difference equations, and it is a discrete analogue of system (37). To find a solution to the difference AP, we will have to solve system (57) for all k , $k = -J, \dots, J$. However, the formulation of the difference AP is still incomplete. To complete it, we have to set some boundary conditions at $m = 0$ and $m = M$ (as was done at $x = 0$ and $x = X$ for the continuous case in section 2.3). These boundary conditions should guarantee the desirable far-field behavior of the solution (i.e., decay at infinity). They will be formulated separately for each wavenumber k , $k = -J, \dots, J$, i.e., the system (eq. (57)) will be supplemented for each k by some boundary conditions at $m = 0$ and $m = M$. The idea for constructing these boundary conditions in the discrete case is analogous to the one implemented in constructing boundary conditions (44) and (45) for continuous system (37). Namely, when formally considered on an infinite one-dimensional mesh, $-\infty < m < \infty$, system (57) obviously becomes homogeneous at least for $m \geq M$ and $m \leq 0$. The homogeneous system has four linearly independent eigensolutions: those that correspond to $|\mu_r^n(k)| < 1$ decrease to the right (i.e., as $m \rightarrow \infty$); those that correspond to $|\mu_r^n(k)| > 1$ decrease to the left (i.e., as $m \rightarrow -\infty$); and those that correspond to $|\mu_r^n(k)| = 1$ have either constant or oscillatory behavior. Here, $\mu_r^n(k)$, $r = 1, \dots, 4$, are the eigenvalues of the matrix $\mathbf{Q}_k^n \stackrel{\text{def}}{=} (\mathbf{A}_k^n)^{-1} \mathbf{B}_k^n$. Let us note that while calculating the eigenvalues $\mu_r(k)$ for the stationary Navier-Stokes equations (ref. 8) (the eigenvalues are calculated numerically using standard NAG subroutines), we have found that for all specific sets of the parameters involved (i.e., grid sizes h_x and h_y and hydrodynamic parameters M_0 , Re , Pr , and γ) the absolute values of eigenvalues were never equal to unity except for the case of zero wavenumber, $k = 0$. For $k = 0$, we have obtained a multiple eigenvalue $|\mu(0)| = 1$. (See ref. 8.) However, even in this case the system matrix still has a basis composed of eigenvectors, which provides us with the reason for not considering the polynomially growing solutions in reference 8. For system (57), we also have a particular case when the eigenvalues of the system matrix become equal to unity in absolute value. Namely, it is easy to see from formula (58) that $\mathbf{Q}_0^0 = (\mathbf{A}_0^0)^{-1} \mathbf{B}_0^0 = -\mathbf{I}$ (identity matrix). Obviously, \mathbf{Q}_0^0 has four linearly independent eigenvectors; therefore, we do not have polynomially growing solutions in this case as well. As for other values of k and n , a numerical check (as was done in ref. 8) will always be necessary to determine whether the eigenvalues $|\mu_r^n(k)| = 1$ exist. If such eigenvalues do exist, a check is also necessary to determine what their multiplicities are and if there is a basis composed of eigenvectors. Relying on our previous experience (ref. 8), we assume that while solving system (57), we can restrict ourselves by considering only these two cases: $|\mu_r^n(k)| \neq 1$ and $|\mu_r^n(k)| = 1$ with the full system of eigenvectors. Nontrivial Jordan blocks (of order more than 1) for $|\mu_r^n(k)| = 1$ are excluded from consideration. Note, if the basis composed of eigenvectors does exist for $|\mu_r^n(k)| = 1$, then system (57) will be treated exactly in the same way as in the case $|\mu_r^n(k)| \neq 1$ (the only difference is that the stability constant becomes proportional to M).

Returning to the question of setting the boundary conditions for system (57) at $m = 0$ and $m = M$, we require that, analogous to the continuous case (see section 2.3), boundary conditions at $m = 0$ should prohibit all modes that do not decrease to the left (i.e., as $m \rightarrow -\infty$) and boundary conditions at $m = M$ should prohibit all modes that increase to the right (i.e., as $m \rightarrow \infty$). Therefore, we may represent the desirable boundary conditions in the form of matrix relations (compare with formulas (44)),

$$\mathbf{S}^{n-}(k)\hat{\mathbf{u}}_{0,k}^n = \mathbf{0} \quad (k = -J, \dots, J) \quad (59a)$$

$$\mathbf{S}^{n+}(k)\hat{\mathbf{u}}_{M,k}^n = \mathbf{0} \quad (k = -J, \dots, J) \quad (59b)$$

where

$$\mathbf{S}^{n-}(k) = \prod_{|\mu_r^n(k)| > 1} (\mathbf{Q}_k^n - \mu_r^n(k)\mathbf{I}) \quad (60a)$$

$$\mathbf{S}^{n+}(k) = \prod_{|\mu_r^n(k)| \leq 1} (\mathbf{Q}_k^n - \mu_r^n(k)\mathbf{I}) \quad (60b)$$

(compare with formulas (45)).

Thus, the final formulation of the difference AP is the following. One should solve the inhomogeneous counterpart to system (52) in D_Y^0 on the grid \mathcal{X}^0 (see formula (53)), where the right-hand side $\hat{\mathbf{f}}_{m+1/2,j}^n$ ($\text{supp} \hat{\mathbf{f}}_{m+1/2,j}^n \subset D_{in}$) is specified on the grid \mathcal{M}^0 (see formula (54)), with periodicity boundary conditions (55) in the y direction and boundary conditions (59a) and (60a) at the line $m = 0$ and (59b) and (60b) at the line $m = M$.

To solve the difference AP, we implement the following numerical procedure. First, apply discrete Fourier transform (56) to both sides of the finite-difference system, then solve the system of ordinary difference equations (57) with boundary conditions (59) for each wavenumber k , $k = -J, \dots, J$, and finally restore the solution by means of the inverse Fourier transform,

$$\hat{\mathbf{u}}_{m,j}^n = \sum_{k=-J}^{k=J} \hat{\mathbf{u}}_{m,k}^n e^{ikjh_y \frac{2\pi}{Y}} \quad (m = 0, 1, \dots, M; j = 0, 1, \dots, 2J) \quad (61)$$

The type of boundary conditions (59) (which are imposed separately for each wavenumber k) makes the choice of numerical method most relevant. An effective algorithm for solving one-dimensional problems (eqs. (57) and (59)) is delineated in our work (ref. 25). We do not reproduce the corresponding results here, we only note that this algorithm may be thought of as a version of the well-known successive substitution technique but without its “inverse” or “resolving” part. The computational cost of the numerical procedure in reference 25 as applied to solving the problem (eqs. (57) and (59)) is $O(M)$ operations (for each k , $k = -J, \dots, J$).

Let us now briefly describe the concept of convergence for the solutions of the difference AP. According to section 2.3, we approximate the nonperiodic solution by a periodic one on a finite interval $-\hat{y} \leq y \leq \hat{y}$ when the period Y grows, $Y \rightarrow \infty$. In its own turn, an approximate solution to the periodic problem is found by a finite-difference method on the grid with sizes h_x and h_y . Therefore, we will consider (uniform) convergence of the periodic difference solution (i.e., solution of the difference AP) to the nonperiodic continuous solution (i.e., to the solution of the original continuous AP) only on a finite rectangle $(0, X) \times (-\hat{y}, \hat{y})$ (this rectangle should be large enough to contain at least Γ_1) rather than on the whole domain of the difference AP. Moreover, we will consider this convergence not only when the grid size vanishes but also when the period Y synchronously increases, i.e., as $(h_x, h_y, Y) \rightarrow (0, 0, \infty)$. Of course, the rate of decrease for the grid sizes h_x and h_y and the rate of increase for the period Y are not independent; some estimates connecting these rates can be found in reference 8. Furthermore, some numerical experiments from reference 8 show that the presented construction of the difference AP does ensure the convergence of its solution to the solution of the continuous AP in the sense just described.

3.3. Computation of ABC's

In accordance with section 2.1, to set the ABC's we need to know the following data: $\left(\hat{\mathbf{u}}_{\mathbf{v}}^n, \frac{\partial \hat{\mathbf{u}}_{\mathbf{v}}^n}{\partial \zeta}\right)$. Here, ζ is the normal to Γ . When integrating the Navier-Stokes equations step-by-step in time, we assume that $\left(\hat{\mathbf{u}}_{\mathbf{v}}^n, \frac{\partial \hat{\mathbf{u}}_{\mathbf{v}}^n}{\partial \zeta}\right)$ is provided from inside D_{in} ; then we use these data to restore $\hat{\mathbf{u}}_{\mathbf{v}_1}^n$, which enables us to advance the next time step. However, as we carry out our analysis in the Fourier space, we cannot consider $\left(\hat{\mathbf{u}}_{\mathbf{v}}^n, \frac{\partial \hat{\mathbf{u}}_{\mathbf{v}}^n}{\partial \zeta}\right)$ as the actual values obtained inside the computational domain. To get $\left(\hat{\mathbf{u}}_{\mathbf{v}}^n, \frac{\partial \hat{\mathbf{u}}_{\mathbf{v}}^n}{\partial \zeta}\right)$, we first have to calculate the Fourier transform of the function $\left(\mathbf{u}_{\mathbf{v}}, \frac{\partial \mathbf{u}_{\mathbf{v}}}{\partial \zeta}\right)$. Without loss of generality, we may always think that the latter is specified at the following points:

$$\mathbf{v} \times \{ \tau l | l = 0, \dots, 2L+1, \tau(2L+1) = T \} \quad (62)$$

Of course, actual discretization in time for the Navier-Stokes equations inside D_{in}^T should not necessarily coincide with the one used for the solution of the exterior linearized problem. (See formula (46)). However, we may always use some interpolation in time to obtain the boundary data on a uniform mesh with respect to t (eq. (62)), which is convenient for further consideration. Hereafter, we simply assume that this interpolation (which is one-dimensional in time and of sufficiently high order) has already been implemented for each node \mathbf{v} , if necessary.

Another important issue related to the step-by-step integration in time is that the function $\left(\mathbf{u}_{\mathbf{v}}, \frac{\partial \mathbf{u}_{\mathbf{v}}}{\partial \zeta}\right)$, which provides the boundary data, is not necessarily time-periodic until we achieve a true oscillatory regime. However, for the purpose of constructing the ABC's, we will propose some generalized treatment of the boundary data as being already periodic. Namely, let us formally calculate the Fourier coefficients of $\left(\mathbf{u}_{\mathbf{v}}, \frac{\partial \mathbf{u}_{\mathbf{v}}}{\partial \zeta}\right)$,

$$\left(\hat{\mathbf{u}}_{\mathbf{v}}^n, \frac{\partial \hat{\mathbf{u}}_{\mathbf{v}}^n}{\partial \zeta}\right) = \frac{1}{2L+1} \sum_{l=1}^{2L+1} \left(\mathbf{u}_{\mathbf{v}}^l, \frac{\partial \mathbf{u}_{\mathbf{v}}^l}{\partial \zeta}\right) e^{-in l \tau \frac{2\pi}{T}} \quad (n = -L, \dots, L) \quad (63)$$

Then, it is well-known (see ref. 24 by Kolmogorov and Fomin) that the time-periodic function

$$\left(\mathbf{v}_{\mathbf{v}}^l, \frac{\partial \mathbf{v}_{\mathbf{v}}^l}{\partial \zeta}\right) = \sum_{n=-L}^L \left(\hat{\mathbf{u}}_{\mathbf{v}}^n, \frac{\partial \hat{\mathbf{u}}_{\mathbf{v}}^n}{\partial \zeta}\right) e^{in l \tau \frac{2\pi}{T}} \quad (l = 0, 1, \dots, 2L+1) \quad (64)$$

minimizes the following functional

$$\left\| \left(\mathbf{u}_{\mathbf{v}}, \frac{\partial \mathbf{u}_{\mathbf{v}}}{\partial \zeta}\right) - \left(\mathbf{v}_{\mathbf{v}}, \frac{\partial \mathbf{v}_{\mathbf{v}}}{\partial \zeta}\right) \right\|_2$$

($\|\cdot\|_2$ is a usual Euclidean norm) on the class of periodic functions; i.e., $\left(\mathbf{v}_v, \frac{\partial \mathbf{v}_v}{\partial \zeta}\right)$ from formula (64) is the best periodic least squares approximation of $\left(\mathbf{u}_v, \frac{\partial \mathbf{u}_v}{\partial \zeta}\right)$. Relying on this property, we will further use Fourier coefficients (63) as the boundary data that “drive” the ABC’s (which may be referred to as the generalized treatment of the boundary data as being time-periodic). Clearly, as we integrate the Navier-Stokes equations in time and approach the true oscillatory regime, the “source” function $\left(\mathbf{u}_v, \frac{\partial \mathbf{u}_v}{\partial \zeta}\right)$ and its Fourier series $\left(\mathbf{v}_v, \frac{\partial \mathbf{v}_v}{\partial \zeta}\right)$ (eq. (64)) also approach each other.

We now implement the DPM (refs. 9 and 10) to actually calculate the ABC’s. We note that the boundary data $\left(\hat{\mathbf{u}}_v^n, \frac{\partial \hat{\mathbf{u}}_v^n}{\partial \zeta}\right)$ are specified on the curve Γ , which is positioned arbitrarily with respect to coordinate lines of the grid \mathcal{X}^0 . (See formula (53).) Moreover, we do not impose any restrictions on the shape of Γ itself. In our opinion, the DPM (refs. 9 and 10) provides an ideal tool for treating such geometrically complicated problems.

Let us introduce the following discrete sets. We consider a six-node two-dimensional stencil

$$St_{m+1/2, j} = \{(x_m, y_j), (x_m, y_{j+1}), (x_m, y_{j-1}), (x_{m+1}, y_j), (x_{m+1}, y_{j+1}), (x_{m+1}, y_{j-1})\}$$

This stencil is actually a projection of the one from figure 6 onto the plane $t = \text{const}$. Obviously, the discretization (52) was obtained using $St_{m+1/2, j}$. Then, we define

$$\mathcal{M}_{in} = \mathcal{M}^0 \cap D_{in} \quad \mathcal{M} = \mathcal{M}^0 \setminus \mathcal{M}_{in} \quad \mathcal{X} = \bigcup_{(x_{m+1/2}, y_j) \in \mathcal{M}} St_{m+1/2, j} \quad \mathcal{X}_{in} = \bigcup_{(x_{m+1/2}, y_j) \in \mathcal{M}_{in}} St_{m+1/2, j} \quad \gamma = \mathcal{X} \cap \mathcal{X}_{in}$$

Clearly, the set of grid nodes γ is located near the artificial boundary Γ . We will call this set *the grid boundary* (by analogy). The sets \mathcal{M}_{in} , \mathcal{M} , \mathcal{X}_{in} , \mathcal{X} , and γ are shown in figure 7.

Further, we will need to interpolate grid functions from \mathcal{X}^0 to the points $\mathbf{v}_1 \subset \Gamma_1$. Let us select all those nodes $\kappa \subset \mathcal{X}^0$ that should be taken into account once constructing local interpolation formulas of sufficiently high (e.g., second) order. All the nodes κ are located not far from Γ_1 . Without loss of generality, we always may assume that $\kappa \subset \mathcal{X}$. We denote the operation of local interpolation from the Cartesian grid \mathcal{X} to \mathbf{v}_1 by $\mathbf{R}_{\mathbf{v}_1, \mathcal{X}}$.

Let us also introduce the set of collocation points $\sigma \subset \Gamma$ and the space of eight-component vector functions $\hat{\mathbf{W}}_\sigma^n \ni \hat{\mathbf{w}}_\sigma^n$ defined on the set σ . The elements of $\hat{\mathbf{W}}_\sigma^n$ will be used as unknowns for the boundary operator equation, which will replace the exterior linear difference problem. Henceforth, we will treat $\hat{\mathbf{w}}_\sigma^n$ as vectors containing the values of \hat{u}^n , \hat{v}^n , \hat{p}^n , and $\hat{\rho}^n$ and the values of the derivatives $\frac{\partial \hat{u}^n}{\partial \zeta}$, $\frac{\partial \hat{v}^n}{\partial \zeta}$, $\frac{\partial \hat{p}^n}{\partial \zeta}$, and $\frac{\partial \hat{\rho}^n}{\partial \zeta}$ at the points σ ; here, ζ is the (outward) normal to Γ . Note that the functions $\hat{\mathbf{w}}_\sigma^n$ are the discrete approximations of $\left(\hat{\mathbf{u}}_v^n, \frac{\partial \hat{\mathbf{u}}_v^n}{\partial \zeta}\right)$ from section 2.1.

Generally, the sizes h_x and h_y of the grid \mathcal{X}^0 and the size h_σ of the one-dimensional collocation grid on the curve Γ are not independent; they should be correlated to each other in a certain way. This requirement is a consequence of convergence conditions for the DPM algorithm. (See ref. 9.) The theoretical questions concerning the correlation between the sizes of grids \mathcal{X}^0 and σ are delineated in

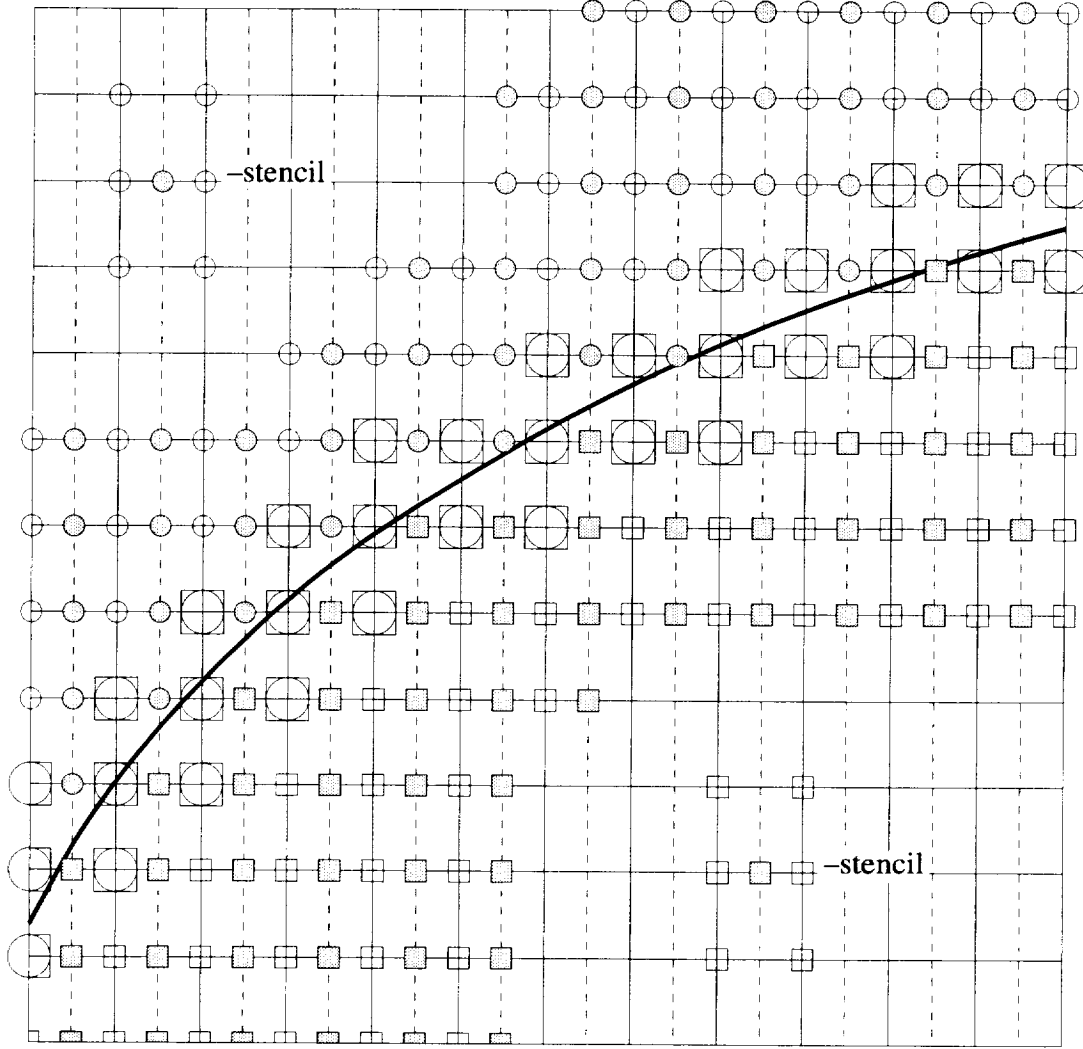


Figure 7. Grid sets. Grid \mathcal{N}^0 —continuous thin vertical lines; \mathcal{M}^0 —continuous thin horizontal lines & dashed thin vertical lines; continuous boundary Γ —thick dark line; \mathcal{M}_{in} —gray boxes; \mathcal{M} —gray circles; \mathcal{N}_{in} —white boxes; \mathcal{N} —white circles; $\gamma = \mathcal{N} \cap \mathcal{N}_{in}$ —big white circles & boxes.

reference 9. As concerns practical applications, the final choice of grids is always done taking into account some previous computational results. In particular, it seems useful to conduct the computations (see refs. 11 and 12) for the set of collocation points, which is more concentrated at the outflow part of the external boundary in the wake region and uniformly spaced at the inflow part of the external boundary. Moreover, sometimes the relation $|\sigma| \sim |\gamma|^{1/2}$ appears to be proper. At any rate, for each specific class of problems (determined both by the geometry of computational domain and by the parameters of fluid at infinity) one always can make an appropriate choice of the grids \mathcal{N}^0 and σ relying on general theory (ref. 9) and on the numerical experience.

Let us now specify some $\hat{\mathbf{w}}_{\sigma}^n \in \hat{\mathbf{W}}_{\sigma}^n$ and implement the following procedure. First, we smoothly interpolate $\hat{\mathbf{w}}_{\sigma}^n$ along Γ (i.e., along the smooth components of Γ) and get the function $\mathbf{R}\hat{\mathbf{w}}_{\sigma}^n$. Here, \mathbf{R} is an interpolation operator. Then, we drop the normals from the points γ to Γ and find the values of $\mathbf{R}\hat{\mathbf{w}}_{\sigma}^n$ at the foots of these normals. Since $\hat{\mathbf{w}}_{\sigma}^n$ (and consequently $\mathbf{R}\hat{\mathbf{w}}_{\sigma}^n$) contains the values of both \hat{u}^n , \hat{v}^n , \hat{p}^n , and $\hat{\rho}^n$ and their normal derivatives and since the distance between any node γ and the curve Γ is small (of order h), we may approximately find \hat{u}^n , \hat{v}^n , \hat{p}^n , and $\hat{\rho}^n$ at the nodes γ using the two first terms of the Taylor expansion. We will designate the entire operation of continuation of the boundary data from

σ to γ as $\pi_{\gamma\sigma}, \pi_{\gamma\sigma} \hat{\mathbf{w}}_\sigma^n = \hat{\mathbf{u}}_\gamma^n$. Note that the preceding algorithm of continuation generally applies to the smooth parts of Γ (where the normal exists). In practice, however, the curve Γ is usually not smooth (see fig. 1), and it is impossible to construct an appropriate normal when the node γ is located in some neighborhood of the breaking point of the curve. The construction of the operator $\pi_{\gamma\sigma}$ in this case is based on the existence of two linearly independent directions along the curve, which enables us to obtain the desirable continuation anyway.

Now, using the calculated continuation of the boundary data, $\hat{\mathbf{u}}_\gamma^n = \pi_{\gamma\sigma} \hat{\mathbf{w}}_\sigma^n$, we construct the following grid function:

$$\hat{\mathbf{u}}_{\mathcal{X}^0}^n \Big|_{m,j} = \begin{cases} \hat{\mathbf{u}}_\gamma^n \Big|_{m,j} & \text{if } (x_m, y_j) \in \gamma \\ \mathbf{0} & \text{if } (x_m, y_j) \in \mathcal{X}^0 \setminus \gamma \end{cases} \quad (65)$$

which is defined already on the entire grid \mathcal{X}^0 . (See formula (53).) Then, we substitute the function $\hat{\mathbf{u}}_{\mathcal{X}^0}^n$ from formula (65) into the left-hand side of system (52). Generally speaking, $\hat{\mathbf{u}}_{\mathcal{X}^0}^n$ does not satisfy equations (52). Therefore, we generate some nonzero right-hand side, which we designate $\mathbf{L}_0^n \hat{\mathbf{u}}_{\mathcal{X}^0}^n$. Here, \mathbf{L}_0^n is the linear operator defined by the left-hand side of system (52). This operator takes the functions defined on the grid \mathcal{X}^0 (eq. (53)) as an input and generates the functions defined on the grid \mathcal{M}^0 (eq. (54)) as a result. Finally, we truncate the function $\mathbf{L}_0^n \hat{\mathbf{u}}_{\mathcal{X}^0}^n$ to the set \mathcal{M}_{in} , which yields

$$\hat{\mathbf{f}}_{\mathcal{M}^0}^n \Big|_{m+1/2,j} = \begin{cases} \mathbf{L}_0^n \hat{\mathbf{u}}_{\mathcal{X}^0}^n \Big|_{m+1/2,j} & \text{if } (x_{m+1/2}, y_j) \in \mathcal{M}_{in} \\ \mathbf{0} & \text{if } (x_{m+1/2}, y_j) \notin \mathcal{M}_{in} \end{cases} \quad (66)$$

We will use the function $\hat{\mathbf{f}}_{\mathcal{M}^0}^n \equiv \hat{\mathbf{f}}_{m+1/2,j}^n$ from formula (66) as the right-hand side for the difference AP; by definition, $\text{supp} \hat{\mathbf{f}}_{m+1/2,j}^n \subset D_{in}$. Once we solve the difference AP with the right-hand side $\hat{\mathbf{f}}_{\mathcal{M}^0}^n$ (eq. (66)), we get the function $\mathbf{G}_0^n \hat{\mathbf{f}}_{\mathcal{M}^0}^n$. Here, \mathbf{G}_0^n is the Green (i.e., inverse) operator of the difference AP. The function $\mathbf{G}_0^n \hat{\mathbf{f}}_{\mathcal{M}^0}^n$ is defined on the grid \mathcal{X}^0 . As it is considered only on the sub-grid $\mathcal{X} \subset \mathcal{X}^0$, it is called *the difference potential* with the density $\hat{\mathbf{u}}_\gamma^n$, $\mathbf{P}_{\mathcal{X}\gamma}^n \hat{\mathbf{u}}_\gamma^n = \mathbf{G}_0^n \hat{\mathbf{f}}_{\mathcal{M}^0}^n \Big|_{\mathcal{X}}$. (See ref. 9.) Clearly, the difference potential satisfies equations (52) since $\hat{\mathbf{f}}_{\mathcal{M}^0}^n = \mathbf{0}$ on \mathcal{M} ; moreover, it satisfies the boundary conditions of the difference AP. The difference potential $\mathbf{P}_{\mathcal{X}\gamma}^n \hat{\mathbf{u}}_\gamma^n$ is a discrete realization of the generalized potential mentioned in the introduction. Later, we will find an approximate (i.e., difference) solution to the problem (eqs. (8)–(10)) in the form of a difference potential and then use this solution to construct the ABC's, i.e., to obtain the missing relations between the unknowns at $\mathbf{v} \subset \Gamma$ and at $\mathbf{v}_1 \subset \Gamma_1$. Therefore, we will need to know the difference potential only on the two subsets of \mathcal{X} located closely to Γ and Γ_1 on $\gamma \subset \mathcal{X}$ and on $\kappa \subset \mathcal{X}$, respectively.

Indeed, once we calculate the difference potential on γ , we can then construct the operator \mathbf{P}_γ^n as the trace of the potential, $\mathbf{P}_\gamma^n \hat{\mathbf{u}}_\gamma^n \stackrel{\text{def}}{=} \mathbf{P}_{\mathcal{X}\gamma}^n \hat{\mathbf{u}}_\gamma^n \Big|_{\gamma}$. This operator will be the key element of the boundary operator equation of the DPM. Actually, \mathbf{P}_γ^n is a difference boundary projection operator (ref. 9), which substitutes \mathbf{P}_Γ^n (see section 2.1, eq. (11)) in practical computations.

Once we calculate the difference potential on κ , we can interpolate it and find the trace of the solution to the linear problem on v_1 , $\hat{\mathbf{u}}_{v_1}^n = \mathbf{P}_{v_1\gamma}^n \hat{\mathbf{u}}_\gamma^n = \mathbf{R}_{v_1\mathcal{N}} \mathbf{P}_{\mathcal{N}\gamma}^n \hat{\mathbf{u}}_\gamma^n$. Thereby, we obtain the desirable relations between the unknowns at Γ and Γ_1 through the solution of the linearized exterior problem. Let us now recall that we have replaced the original infinite-in-space problem by the periodic problem formulated on the strip $\{-\infty < x < \infty\} \times \left\{-\frac{Y}{2} \leq y \leq \frac{Y}{2}\right\}$, claiming that we will need to know the solution only on some neighborhood of D_{in} , and therefore the convergence on a fixed interval, $-\hat{y} \leq y \leq \hat{y}$, is sufficient for our purposes (see subsection 2.3). Since we do not need to calculate the difference potential anywhere except at γ and κ , the previous statement is now justified.

We now formulate the main result of the DPM theory. (See ref. 9.) Consider the entire space of grid functions $\hat{\mathbf{u}}_\gamma^n$ defined on γ . Those and only those elements of this space which satisfy the equation

$$\mathbf{P}_\gamma^n \hat{\mathbf{u}}_\gamma^n = \hat{\mathbf{u}}_\gamma^n \quad (67)$$

can be complemented to \mathcal{N} so that the complement solves system (52) (with boundary conditions (55) and (59)). As previously mentioned, the operator \mathbf{P}_γ^n is a projection; it is a discrete analogue of the Calderon boundary pseudodifferential operators. (See ref. 17.) For any $\hat{\mathbf{u}}_\gamma^n$, the result $\mathbf{P}_\gamma^n \hat{\mathbf{u}}_\gamma^n$ (as well as $\mathbf{P}_{v_1\gamma}^n \hat{\mathbf{u}}_\gamma^n$) can be explicitly calculated in accordance with the aforementioned procedure, $\hat{\mathbf{u}}_\gamma^n \Rightarrow \hat{\mathbf{u}}_{\mathcal{N}^0}^n \Rightarrow \mathbf{L}_0^n \hat{\mathbf{u}}_{\mathcal{N}^0}^n \Rightarrow \hat{\mathbf{f}}_{\mathcal{M}^0}^n \Rightarrow \mathbf{G}_0^n \hat{\mathbf{f}}_{\mathcal{M}^0}^n \Rightarrow \mathbf{P}_{\mathcal{N}\gamma}^n \hat{\mathbf{u}}_\gamma^n \Rightarrow \mathbf{P}_\gamma^n \hat{\mathbf{u}}_\gamma^n, \mathbf{P}_{v_1\gamma}^n \hat{\mathbf{u}}_\gamma^n$.

In section 2.1, we have declared our goal as to characterize those and only those $\left(\hat{\mathbf{v}}_\Gamma^n, \frac{\partial \hat{\mathbf{v}}_\Gamma^n}{\partial \zeta}\right)$ that would solve equations (8) with boundary conditions (9) on D_{ex} and coincide with the trace of the solution on Γ . Instead, we have provided an analogous classification (see eq. (67)) for the discrete rather than for the continuous formulation of the problem. Therefore, we have equivalently replaced linear system (52) on \mathcal{N} , along with the boundary conditions (55) and (59), by the boundary equation with projection (eq. (67)). Consequently, we can now specify the proper boundary data (see equality (10)) for the discrete counterpart of the problem (eqs. (8)–(10)). Namely, let us take any $\left(\hat{\mathbf{u}}_v^n, \frac{\partial \hat{\mathbf{u}}_v^n}{\partial \zeta}\right)$ (provided from inside D_{in}) and interpolate it along Γ to the set of collocation points σ , $\hat{\mathbf{w}}_\sigma^n = \mathbf{R}_{\sigma v} \left(\hat{\mathbf{u}}_v^n, \frac{\partial \hat{\mathbf{u}}_v^n}{\partial \zeta}\right)$. Then, continue $\hat{\mathbf{w}}_\sigma^n$ using the operator $\pi_{\gamma\sigma}$, and finally apply \mathbf{P}_γ^n (which requires solving the AP). In accordance with the previously formulated main result, the grid function

$$\hat{\mathbf{v}}_\gamma^n = \mathbf{P}_\gamma^n \pi_{\gamma\sigma} \mathbf{R}_{\sigma v} \left(\hat{\mathbf{u}}_v^n, \frac{\partial \hat{\mathbf{u}}_v^n}{\partial \zeta}\right) \quad (68)$$

admits the complement to \mathcal{N} that solves the problem (eqs. (52), (55), and (59)).

Thus, we have completed the first stage of constructing the ABC's (section 2.1) and now proceed to the second one. Instead of the problem (eqs. (8)–(10)), we will consider its discrete counterpart: to solve system (52) on \mathcal{N} with external boundary conditions (55) and (59), and with boundary condition

$$\hat{\mathbf{u}}_{\gamma}^n = \hat{\mathbf{v}}_{\gamma}^n \quad (69)$$

at γ ; $\hat{\mathbf{v}}_{\gamma}^n$ in equality (69) comes from formula (68). The solvability of the problem (eqs. (52), (55), (59), and (69)) is guaranteed by the special type of boundary data provided in formula (68).

To actually find the solution to the problem (eqs. (52), (55), (59), and (69)), we calculate the difference potential $\mathbf{P}_{\mathcal{A}\gamma}^n \hat{\mathbf{v}}_{\gamma}^n$ with the density $\hat{\mathbf{v}}_{\gamma}^n$ from formula (68). Then, we interpolate the potential from \mathcal{A} to \mathbf{v}_1 , which yields

$$\hat{\mathbf{u}}_{\mathbf{v}_1}^n = \mathbf{R}_{\mathbf{v}_1, \mathcal{A}} \mathbf{P}_{\mathcal{A}\gamma}^n \mathbf{P}_{\gamma}^n \pi_{\gamma\sigma} \mathbf{R}_{\sigma\mathbf{v}} \left(\hat{\mathbf{u}}_{\mathbf{v}}^n, \frac{\partial \hat{\mathbf{u}}_{\mathbf{v}}^n}{\partial \zeta} \right) \stackrel{def}{=} \hat{\mathbf{T}}^n \left(\hat{\mathbf{u}}_{\mathbf{v}}^n, \frac{\partial \hat{\mathbf{u}}_{\mathbf{v}}^n}{\partial \zeta} \right) \quad (70)$$

Equality (70) provides the missing relations between the unknowns at \mathbf{v} and at \mathbf{v}_1 in the Fourier space; these relations are based on the solution to the linearized exterior problem. Therefore, equality (70) is almost the desirable ABC, and the only remaining step is the inverse Fourier transform in time. Before implementing the inverse transform, let us note that the entire algorithm becomes most convenient from a practical standpoint if we calculate the matrix representation of the operator $\hat{\mathbf{T}}^n$ from formula (70). To do that, we choose some basis in $\hat{\mathbf{W}}_{\sigma}^n$, e.g., the simplest one, composed of the vectors like $(0, \dots, 0, 1, 0, \dots, 0)$, and implement the entire proceeding procedure. More precisely, we calculate $\hat{\mathbf{u}}_{\mathbf{v}_1}^n = \mathbf{R}_{\mathbf{v}_1, \mathcal{A}} \mathbf{P}_{\mathcal{A}\gamma}^n \mathbf{P}_{\gamma}^n \pi_{\gamma\sigma} \hat{\mathbf{w}}_{\sigma}^n$, for each basis vector $\hat{\mathbf{w}}_{\sigma}^n$. In so doing, we obtain the matrix of $\mathbf{R}_{\mathbf{v}_1, \mathcal{A}} \mathbf{P}_{\mathcal{A}\gamma}^n \mathbf{P}_{\gamma}^n \pi_{\gamma\sigma}$ (each column will be the response to a specific basic function $\hat{\mathbf{w}}_{\sigma}^n$) and then, multiplying the above matrix from the right by the interpolation matrix $\mathbf{R}_{\sigma\mathbf{v}}$, we finally obtain the matrix representation of $\hat{\mathbf{T}}^n$.

(Note that we do not start from basis functions $\left(\hat{\mathbf{u}}_{\mathbf{v}}^n, \frac{\partial \hat{\mathbf{u}}_{\mathbf{v}}^n}{\partial \zeta} \right)$ since the number of nodes σ is usually much less than the number of nodes \mathbf{v} .) In fact, it is possible to show (see ref. 9) that for any $\hat{\mathbf{w}}_{\sigma}^n$, $\mathbf{P}_{\mathcal{A}\gamma}^n \mathbf{P}_{\gamma}^n \pi_{\gamma\sigma} \hat{\mathbf{w}}_{\sigma}^n \equiv \mathbf{P}_{\mathcal{A}\gamma}^n \pi_{\gamma\sigma} \hat{\mathbf{w}}_{\sigma}^n$ and therefore we need to calculate the matrix $\mathbf{R}_{\mathbf{v}_1, \mathcal{A}} \mathbf{P}_{\mathcal{A}\gamma}^n \pi_{\gamma\sigma}$. Clearly, the computation of each column of the matrix $\mathbf{R}_{\mathbf{v}_1, \mathcal{A}} \mathbf{P}_{\mathcal{A}\gamma}^n \pi_{\gamma\sigma}$ requires one solution of the difference AP, which, in turn, involves the direct (eq. (56b)) and inverse (eq. (61)) Fourier transforms and the solution of the problem (eqs. (57) and (59)) for each wavenumber k , $k = -J, \dots, J$. Either Fourier transform will require only $O(M \cdot J)$ rather than $O(M \cdot J^2)$ operations. (For definitions of M and J , see formula (46).) Indeed, the support of the right-hand side $\hat{\mathbf{f}}_{\mathcal{A}0}^n$ is actually concentrated near Γ since $\hat{\mathbf{u}}_{\mathcal{A}0}^n$ differs from zero only on γ and the operator \mathbf{L}_0^n is local. Therefore, while calculating direct Fourier transform (56b) for each m , $m = 0, 1, \dots, M-1$, only a few values $\hat{\mathbf{f}}_{m+1/2, j}^n$ differ from zero, and consequently the total cost of this computation is $O(M \cdot J)$ operations. Analogously, while calculating the inverse Fourier transform (61) for each m , $m = 0, 1, \dots, M$, we need to know $\hat{\mathbf{u}}_{m, j}^n$ only for a few selected values of j since all other (x_m, y_j) do not belong to κ . Therefore, the total cost of this computation is $O(M \cdot J)$ operations as well. Finally, the solution of the problem (eqs. (57) and (59)) for each wavenumber k , $k = -J, \dots, J$ costs $O(M)$ operations. (See ref. 24.) Adding all these quantities, we obtain a total of $O(M \cdot J)$ operations for the computation of each column of the matrix $\mathbf{R}_{\mathbf{v}_1, \mathcal{A}} \mathbf{P}_{\mathcal{A}\gamma}^n \pi_{\gamma\sigma}$. We see that although the entire algorithm requires repeated solution of the difference AP, the solution may be obtained by means of an efficient procedure, which should make the total expense for calculating the

ABC's quite acceptable. Note that in our previous work (see refs. 8, 11, and 12) we have used a different version of the algorithm. We expect that the total cost per one Fourier mode in time will decrease for the current version because of using the thin-layer rather than the full Navier-Stokes equations. (Indeed, the matrices \mathbf{A}_k^n and \mathbf{B}_k^n in system (57) are 4×4 and the matrices for the full Navier-Stokes equations are 8×8 .) (See ref. 8.)

Recall, our final goal is to express the values of physical variables at \mathbf{v}_1 , $\mathbf{u}_{\mathbf{v}_1} \equiv (u_{\mathbf{v}_1}, v_{\mathbf{v}_1}, p_{\mathbf{v}_1}, \rho_{\mathbf{v}_1})$, in terms of $\left(\mathbf{u}_{\mathbf{v}}, \frac{\partial \mathbf{u}_{\mathbf{v}}}{\partial \zeta} \right)$. Choosing the same discretization in time as in the formula (eq. (62)) and implementing inverse Fourier transform (64), we obtain from formula (70),

$$\mathbf{u}_{\mathbf{v}_1}^l = \sum_{n=-L}^{n=L} \hat{\mathbf{T}}^n \left(\hat{\mathbf{u}}_{\mathbf{v}}^n, \frac{\partial \hat{\mathbf{u}}_{\mathbf{v}}^n}{\partial \zeta} \right) e^{inl\tau \frac{2\pi}{T}} \quad (l = 0, 1, \dots, 2L+1) \quad (71)$$

Then, substituting expression (63) into formula (71) and changing the summation order, we get,

$$\begin{aligned} \mathbf{u}_{\mathbf{v}_1}^l &= \sum_{n=-L}^{n=L} \hat{\mathbf{T}}^n e^{inl\tau \frac{2\pi}{T}} \frac{1}{2L+1} \sum_{s=1}^{2L+1} \left(\mathbf{u}_{\mathbf{v}}^s, \frac{\partial \mathbf{u}_{\mathbf{v}}^s}{\partial \zeta} \right) e^{-ins\tau \frac{2\pi}{T}} \\ &= \frac{1}{2L+1} \sum_{n=-L}^{n=L} \sum_{s=1}^{2L+1} \hat{\mathbf{T}}^n e^{inl\tau \frac{2\pi}{T}} \left(\mathbf{u}_{\mathbf{v}}^s, \frac{\partial \mathbf{u}_{\mathbf{v}}^s}{\partial \zeta} \right) e^{-ins\tau \frac{2\pi}{T}} \\ &= \sum_{s=1}^{2L+1} \left(\frac{1}{2L+1} \sum_{n=-L}^{n=L} e^{in(l-s)\tau \frac{2\pi}{T}} \hat{\mathbf{T}}^n \right) \left(\mathbf{u}_{\mathbf{v}}^s, \frac{\partial \mathbf{u}_{\mathbf{v}}^s}{\partial \zeta} \right) \end{aligned}$$

Finally, designating

$$\mathbf{T}^{l,s} = \left(\frac{1}{2L+1} \sum_{n=-L}^{n=L} e^{in(l-s)\tau \frac{2\pi}{T}} \hat{\mathbf{T}}^n \right) \quad (l = 0, 1, \dots, 2L+1)$$

we obtain

$$\mathbf{u}_{\mathbf{v}_1}^l = \sum_{s=1}^{2L+1} \mathbf{T}^{l,s} \left(\mathbf{u}_{\mathbf{v}}^s, \frac{\partial \mathbf{u}_{\mathbf{v}}^s}{\partial \zeta} \right) \quad (l = 0, 1, \dots, 2L+1) \quad (72)$$

Equality (72), which is a specification of equality (11), provides the missing boundary relations between the values of the unknowns at Γ^T and at Γ_1^T (in the discrete formulation). Therefore, equality (72) provides the ABC's we were aiming to obtain. Additionally, we note that the ABC's (eq. (72)) can be simplified for the case of integrating the Navier-Stokes equations step-by-step in time inside D_{in} . In doing so, we only need to know $\mathbf{u}_{\mathbf{v}_1}$ on the upper time level, i.e., for $t = T$, which corresponds to $l = 2L+1$ or to $l = 0$ because of the periodicity. Substituting $l = 0$ into equality (72), we obtain

$$\mathbf{u}_{\mathbf{v}_1} \Big|_{t=T} = \sum_{s=1}^{2L+1} \mathbf{T}^{0,s} \left(\mathbf{u}_{\mathbf{v}}^s, \frac{\partial \mathbf{u}_{\mathbf{v}}^s}{\partial \zeta} \right) \quad (73)$$

Equality (73) is a desirable global ABC for implementation together with the step-by-step integration procedure in time. Indeed, formula (73) expresses the values of u , v , p , and ρ (perturbations) at the

outermost coordinate row v_1 on the upper time level $t = T$ as a function of the prescribed data $\left(\mathbf{u}_v, \frac{\partial \mathbf{u}_v}{\partial \zeta} \right)$ through the time-periodic solution of the linearized thin-layer equations with the free-stream boundary condition at infinity. We note that the matrices of operators $\mathbf{T}^{0,s}$ are calculated explicitly and therefore, the practical implementation of the ABC's (eq. (73)) is reduced to a few matrix-vector multiplications. We also note that this practical implementation may preliminarily require some interpolation in time at the nodes v , which may be represented in a matrix form as well. If we use an explicit scheme for integrating the Navier-Stokes equations inside D_{in} , then we directly implement formula (73) at each time step for determining the missing values of the unknowns at the outermost coordinate row of the grid on the upper time level. If the scheme inside D_{in} is implicit, then we include the relations (eq. (73)) into the system of equations we solve on the upper time level treating all $\mathbf{T}^{0,s} \left(\mathbf{u}_v^s, \frac{\partial \mathbf{u}_v^s}{\partial \zeta} \right)$ for $s < 2L + 1$ as forcing terms.

4. Concluding Remarks

We have constructed the DPM-based nonlocal artificial boundary conditions for computation of oscillating external flows, specifically, compressible viscous fluid flows past finite bodies. To develop the ABC's, we used linearization of the governing equations against the constant free-stream background in the far field. To justify the constructions of difference potentials used for computation of the ABC's, we provided some results on solvability of the linearized thin-layer equations. The nonlocal nature of the proposed ABC's arises from their closeness to the exact boundary conditions. In spite of this nonlocal nature, our ABC's apply to artificial boundaries of irregular shape with equal ease, which is very important for applications. We expect that these boundary conditions may become an effective numerical tool in practical computing. The numerical results on the implementation of the described ABC's will be presented in future work.

Note that we describe the algorithm for calculating the ABC's only for a particular class of methods used for integrating the Navier-Stokes equations inside D_{in} , namely, for such methods that the knowledge of missing relations between only two external coordinate rows of the grid (v and v_1) is sufficient for closing the discrete system inside the computational domain. Obviously, once the method used inside D_{in} is of higher (than the second) order, the consideration of only two curves, Γ and Γ_1 , might be insufficient. However, we always can assume that the "linear region" D_{ex} contains more than one curve, e.g., Γ_1 and Γ_2 instead of only Γ_1 , and can treat this case in the same way as described in this paper. Moreover, one can use higher order schemes for solving the linearized exterior problem as well. Such modifications may extend the possible range of applications for the described technique by including, for example, some computational problems of aeroacoustics.

NASA Langley Research Center
Hampton, VA 23681-0001
April 11, 1996

References

1. Givoli, Dan: Non-Reflecting Boundary Conditions. *J. Comput. Phys.*, vol. 94, May 1991, pp. 1–29.
2. Givoli, Dan: *Numerical Methods for Problems in Infinite Domains*. Elsevier, 1992.
3. Gustafsson, Bertil: Far Field Boundary Conditions for Time-Dependent Hyperbolic Systems. *SIAM J. Sci. Stat. Comput.*, vol. 9, no. 5, Sept. 1988, pp. 812–828.
4. Gustafsson, B.: The Choice of Numerical Boundary Conditions for Hyperbolic Systems. *J. Comput. Phys.*, vol. 48, Nov. 1982, pp. 270–283.

5. Gustafsson, Bertil: Inhomogeneous Conditions at Open Boundaries for Wave Propagation Problems. *Appl. Numer. Math.*, vol. 4, Mar. 1988, pp. 3–19.
6. Carpenter, Mark H.; Gottlieb, David; and Abarbanel, Saul: Time-Stable Boundary Conditions for Finite-Difference Schemes Solving Hyperbolic Systems: Methodology and Application to High-Order Compact Schemes. *J. Comput. Phys.*, vol. 111, no. 2, Apr. 1994, pp. 220–236.
7. Seifert, A.; Daraby, A.; Nishri, B.; and Wygnanski, I.: The Effects of Forced Oscillations on the Performance of Airfoils. AIAA-93-3264, July 1993.
8. Ryaben'kii, V. S.; and Tsynkov, S. V.: Artificial Boundary Conditions for the Numerical Solution of External Viscous Flow Problems. *SIAM J. Numer. Anal.*, vol. 32, no. 5, 1995, pp. 1355–1389.
9. Ryaben'kii, Viktor Solomonovich: The Difference Potential Method for Some Problems in Continuum Mechanics. *Izdatel'stvo Nauka*, (Moscow), 1987.
10. Ryaben'kii, V. S.: Boundary Equations With Projections. *Russian Math. Surv.*, vol. 40, no. 2, 1985, p. 121–183.
11. Tsynkov, S. V.: An Application of Nonlocal External Conditions to Viscous Flow Computations. *J. Comp. Phys.*, vol. 116, no. 2, 1995, p. 212–225.
12. Tsynkov, S. V.; Turkel, E.; and Abarbanel, S.: External Flow Computations Using Global Boundary Conditions. *AIAA J.*, vol. 34, no. 4, Apr. 1996, pp. 700–706.
13. Jameson, A.; Schmidt, Wolfgang; and Turkel, Eli: Numerical Solution of the Euler Equations by Finite Volume Methods Using Runge Kutta Time Stepping Schemes. AIAA-81-1259, June 1981.
14. Swanson, R. C.; and Turkel, Eli: A Multistage Time-Stepping Scheme for the Navier-Stokes Equations. AIAA-85-0035, Jan. 1985.
15. Swanson, R. C.; and Turkel, Eli: Artificial Dissipation and Central Difference Schemes for the Euler and Navier-Stokes Equations. AIAA-87-1107, June 1987.
16. Ryaben'kii, V. S.: Exact Transfer of Boundary Conditions. *Comp. Mech. Solids*, Issue 1, 1990, pp. 129–145.
17. Calderon, A. P.: Boundary-Value Problems for Elliptic Equations. *Proceedings of the Joint Soviet-American Symposium on Partial Differential Equations*, Novosibirsk, Aug. 1963, p. 303–304.
18. Anderson, Dale A.; Tannehill, John C.; and Pletcher, Richard H.: *Computational Fluid Mechanics and Heat Transfer*. Hemisphere Publ. Corp., 1984.
19. Hörmander, L.: *Linear Partial Differential Operators*. Springer, 1963.
20. Vladimirov, V. S.: *Equations of Mathematical Physics*. M. Dekker, 1971.
21. Wolfram, Stephen: *MathematicaTM—A System for Doing Mathematics by Computer*. Addison-Wesley Publ. Co., Inc., 1991.
22. Walker, Robert John: *Algebraic Curves*. Princeton Univ. Press, 1950.
23. Vainberg, B. R.: Some Problems for Hypo-Elliptic Equations Which are Well-Posed in the Entire Plane. *Mat. Sb.*, vol. 62, no. 104, 1963, p. 186–248.
24. Kolmogorov, A. N.; and Fomin, S. V.: *Elements of the Theory of Functions and Functional Analysis*, *Nauka*, (Moscow), 1981.
25. Ryaben'kii, V. S.; and Tsynkov, S. V.: An Effective Numerical Technique for Solving a Special Class of Ordinary Difference Equations. *Appl. Numer. Math.*, vol. 18, no. 4, Oct. 1995, pp. 489–501.

REPORT DOCUMENTATION PAGE			Form Approved OMB No. 0704-0188	
Public reporting burden for this collection of information is estimated to average 1 hour per response, including the time for reviewing instructions, searching existing data sources, gathering and maintaining the data needed, and completing and reviewing the collection of information. Send comments regarding this burden estimate or any other aspect of this collection of information, including suggestions for reducing this burden, to Washington Headquarters Services, Directorate for Information Operations and Reports, 1215 Jefferson Davis Highway, Suite 1204, Arlington, VA 22202-4302, and to the Office of Management and Budget, Paperwork Reduction Project (0704-0188), Washington, DC 20503.				
1. AGENCY USE ONLY (Leave blank)	2. REPORT DATE August 1996	3. REPORT TYPE AND DATES COVERED Technical Memorandum		
4. TITLE AND SUBTITLE Artificial Boundary Conditions for Computation of Oscillating External Flows			5. FUNDING NUMBERS WU 505-59-53-01	
6. AUTHOR(S) S. V. Tsynkov				
7. PERFORMING ORGANIZATION NAME(S) AND ADDRESS(ES) NASA Langley Research Center Hampton, VA 23681-0001			8. PERFORMING ORGANIZATION REPORT NUMBER L-17513	
9. SPONSORING/MONITORING AGENCY NAME(S) AND ADDRESS(ES) National Aeronautics and Space Administration Washington, DC 20546-0001			10. SPONSORING/MONITORING AGENCY REPORT NUMBER NASA TM-4714	
11. SUPPLEMENTARY NOTES Tsynkov: NRC-NASA Resident Research Associate, Langley Research Center, Hampton, VA.				
12a. DISTRIBUTION/AVAILABILITY STATEMENT Unclassified-Unlimited Subject Category 02 Availability: NASA CASI (301) 621-0390			12b. DISTRIBUTION CODE	
13. ABSTRACT (Maximum 200 words) In this paper, we propose a new technique for the numerical treatment of external flow problems with oscillatory behavior of the solution in time. Specifically, we consider the case of unbounded compressible viscous plane flow past a finite body (airfoil). Oscillations of the flow in time may be caused by the time-periodic injection of fluid into the boundary layer, which in accordance with experimental data, may essentially increase the performance of the airfoil. To conduct the actual computations, we have to somehow restrict the original unbounded domain, that is, to introduce an artificial (external) boundary and to further consider only a finite computational domain. Consequently, we will need to formulate some artificial boundary conditions (ABC's) at the introduced external boundary. The ABC's we are aiming to obtain must meet a fundamental requirement. One should be able to uniquely complement the solution calculated inside the finite computational domain to its infinite exterior so that the original problem is solved within the desired accuracy. Our construction of such ABC's for oscillating flows is based on an essential assumption: the Navier-Stokes equations can be linearized in the far field against the free-stream background. To actually compute the ABC's, we represent the far-field solution as a Fourier series in time and then apply the Difference Potentials Method (DPM) of V. S. Ryaben'ki. This paper contains a general theoretical description of the algorithm for setting the DPM-based ABC's for time-periodic external flows. Based on our experience in implementing analogous ABC's for steady-state problems (a simpler case), we expect that these boundary conditions will become an effective tool for constructing robust numerical methods to calculate oscillatory flows.				
14. SUBJECT TERMS Time-periodic flows; Artificial boundary conditions; Boundary projection operators; Difference potentials method			15. NUMBER OF PAGES 44	
			16. PRICE CODE A03	
17. SECURITY CLASSIFICATION OF REPORT Unclassified	18. SECURITY CLASSIFICATION OF THIS PAGE Unclassified	19. SECURITY CLASSIFICATION OF ABSTRACT Unclassified	20. LIMITATION OF ABSTRACT	